Ferroptosis Integrates Mitochondrial Derangements and Pathological Inflammation to Promote Pulmonary Hypertension

Felipe Kazmirczak, MD[1*], Neal T. Vogel, MS[2*], Sasha Z. Prisco, MD, PhD[2*], Michael T. Patterson, PhD[3], Jeffrey Annis, PhD[4], Ryan T. Moon, BS[2], Lynn M Hartweck, PhD[2], Jenna B. Mendelson, BS[2], Minwoo Kim, BS[2], Natalia Calixto Mancipe, PhD[5], Todd Markowski, BS[6], LeAnn Higgins, PhD[6], Candace Guerrero, PhD[6], Ben Kremer, BS[2], Madelyn L. Blake, BS[2], Christopher J. Rhodes, PhD[7], Jesse W. Williams, PhD[3,8], Evan L. Brittain, MD, MSCI[4], and Kurt W. Prins, MD, PhD[2]

* indicates equal contribution

1. Minneapolis Heart Institute, Minneapolis, MN
2. Lillehei Heart Institute, Cardiovascular Division, Department of Medicine, University of Minnesota, Minneapolis, MN
3. Center for Immunology, University of Minnesota, Minneapolis, Minnesota
4. Division of Cardiovascular Medicine, Department of Medicine, Vanderbilt University Medical Center, Nashville, TN
5. Minnesota Supercomputing Institute, University of Minnesota, Minneapolis, MN
6. Center for Metabolomics and Proteomics, Department of Biochemistry, Molecular Biology, and Biophysics, University of Minnesota
7. National Heart and Lung Institute, Imperial College, London, UK
8. Department of Integrative Biology and Physiology, University of Minnesota, Minneapolis, Minnesota

Short Title: Ferroptosis Promotes Pulmonary Hypertension

Author for Correspondence

Kurt W. Prins, MD, PhD

Associate Professor of Medicine

Director of Translational Research in Pulmonary Hypertension

Lillehei Heart Institute

Department of Medicine, University of Minnesota

Abstract

Background: Mitochondrial dysfunction, characterized by impaired lipid metabolism and heightened reactive oxygen species (ROS) generation, results in lipid peroxidation and ferroptosis. Ferroptosis is an inflammatory mode of cell death that promotes complement activation and macrophage recruitment. In pulmonary arterial hypertension (PAH), pulmonary arterial endothelial cells (PAEC) exhibit cellular phenotypes that promote ferroptosis. Moreover, there is ectopic complement deposition and inflammatory macrophage accumulation in the pulmonary vasculature. However, the effects of ferroptosis inhibition on these pathogenic mechanisms and the cellular landscape of the pulmonary vasculature are incompletely defined.

Methods: Multi-omics and physiological analyses evaluated how ferroptosis inhibition modulated preclinical PAH. The impact of AAV1-mediated expression of the pro-ferroptotic protein ACSL4 on PAH was determined, and a genetic association study in humans further probed the relationship between ferroptosis and pulmonary hypertension (PH).

Results: Ferrostatin-1, a small-molecule ferroptosis inhibitor, mitigated PAH severity in monocrotaline rats. RNA-seq and proteomics analyses demonstrated ferroptosis was associated with PAH severity. RNA-seq, proteomics, and confocal microscopy revealed complement activation and pro-inflammatory cytokines/chemokines were suppressed by ferrostatin-1. Additionally, ferrostatin-1 combatted changes in endothelial, smooth muscle, and interstitial macrophage abundance and gene activation patterns as revealed by deconvolution RNA-seq. Ferroptotic PAEC damage associated molecular patterns restructured the transcriptomic signature, mitochondrial morphology, and promoted proliferation of pulmonary artery smooth muscle cells, and created a pro-inflammatory phenotype in monocytes *in vitro*. AAV1-*Acsl4* induced an inflammatory PAH phenotype in rats. Finally, single-nucleotide polymorphisms in six ferroptosis genes identified a potential link between ferroptosis and PH severity in the Vanderbilt BioVU repository.

Conclusions: Ferroptosis promotes PAH through metabolic and inflammatory mechanisms in the pulmonary vasculature.

Non-standard Abbreviations and Acronyms

AAV: Adeno-associated virus

ACSL: Acyl-CoA synthetase long-chain

AKT: AKT serine/threonine kinase

CD80: Cluster of differentiation 80

CD86: Cluster of differentiation 86

CD209: Cluster of differentiation 209

Ea: Effective arterial elastance

Ees/Ea: Ratio of End-systolic elastance/effective arterial elastance

CCL: C-C motif chemokine ligands

CXCL: C-X-C motif chemokine ligands

DAMP: Damage associated molecular patterns

DAPI: 6-diamidino-2-phenylindole

GFP: Green fluorescent protein

HIF: Hypoxia inducible factor

HMOX: Heme oxygenase 1

KEGG: Kyoto encyclopedia of genes and genomes

LPC: Lysophosphatidylcholines

LPE: Lysophosphatidylethanolamine

LPS: Lysophosphatidylserine

MCT: Monocrotaline

MerTK: Mer proto-oncogen, tyrosine kinase

mPAP: Mean pulmonary arterial pressure

MS: Mass spectrometry

NLRP3: NOD-, LRR-, and pyrin domain-containing protein 3

NODAL: Nodal growth differentiation factor

PAEC: Pulmonary arterial endothelial cell

PAH: Pulmonary arterial hypertension

PH: Pulmonary hypertension

PASMC: Pulmonary artery smooth muscle cells

PC: Phosphatidylcholines

PCBP2: Poly(rC)-binding protein 2

PE: Phosphatidylethanolamine

PI3K: Phosphoinositide 3-kinase

PS: Phosphatidylserine

PVR: Pulmonary vascular resistance

RNA-seq: RNA-sequencing

ROS: Reactive oxygen species

RV: Right ventricular/right ventricle

RVSP: Right ventricular systolic pressure

SNP: Single-nucleotide polymorphisms

TAPSE: Tricuspid annular plane systolic excursion

VDAC: Voltage-dependent anion-selective channel

VEH: Vehicle

Introduction

The accumulation of iron-dependent lipid peroxides induces ferroptosis, a nonapoptotic form of cell death that integrates metabolic derangements, oxidative stress, and inflammation[1]. Multiple organelles regulate ferroptosis, but the mitochondria may be the most important because mitochondria both initiate and propagate ferroptosis[1]. Altered ferroptosis homeostasis occurs in multiple disease states including cancer, sepsis, cardiovascular diseases, and aging, showing the broad implications this mode of cell death has in medicine[1]. The discovery of ferrostatin-1[2] and liproxstatin-1[3], two small molecule inhibitors of ferroptosis, greatly expanded our knowledge of ferroptosis as these molecules exert therapeutic effects in a wide-array of conditions[1]. In the systemic vasculature, ferroptosis induces endothelial cell dysfunction and accelerates atherosclerosis development in mice, and importantly this is suppressed by ferrostatin-1 treatment[4]. In pulmonary arterial hypertension (PAH), pulmonary arterial endothelial cell (PAEC) dysfunction, characterized by disrupted mitochondrial function and impaired iron and lipid metabolism[5], sets up a pro-ferroptotic environment. This hypothesis is supported by the observation that small molecule and genetic interventions that suppress ferroptosis reduce PAH severity in rodents[6-8]. However, the timing and therapeutic potential of antagonizing ferroptosis in PAH requires further investigation. Certainly, previous rodent studies show ferroptosis suppression reduces PAH severity, but these studies intervene with ferrostatin-1 immediately before monocrotaline injection[6] or lenti-virus mediated overexpression of the anti-ferroptotic protein peroxiredoxin-6 72 hours prior to monocrotaline injection[7]. At present, the impact of ferroptosis inhibition on pathological pulmonary vascular remodeling after PAH has developed are unknown, and this has important translational implications for treating PAH with ferroptosis suppressing approaches.

In addition to being driven by disrupted metabolism, ferroptosis could promote adverse pulmonary vascular remodeling via modulation of the innate immune system and signaling to surrounding cells in the pulmonary vasculature. Ferroptotic cells release damage associated molecular patterns (DAMPs)[9], which promote ectopic complement deposition[10], a finding present in rodent and human PAH[11]. DAMPs also recruit monocyte derived macrophages to areas of tissue damage[12], which can further amplify the deleterious pro-inflammatory state. In rodent and human PAH, monocyte-derived inflammatory interstitial macrophage numbers are increased in the pulmonary vasculature, and blocking interstitial macrophage invasion into the lungs reduces PAH severity[13]. At present, the direct effects of ferroptotic PAEC DAMPs on macrophage/monocyte biology are unknown.

Moreover, the impact of ferroptotic DAMPs on pulmonary artery smooth muscle cells (PASMC), a cell type that regulates pulmonary vascular disease due to heightened proliferation and increased contractility[14], pathophysiology are unexplored.

To address these important unknowns, we employed mechanistic and translational studies using cell culture-based experiments, physiological and multi-omics evaluations in rodents, and a genetics association study in humans to define the role of ferroptosis in PAH. In particular, we performed a drug intervention rodent study and used quantitative lung proteomics, bulk and deconvolution RNA-sequencing, histological examinations, and lung metabolomics to evaluate how ferroptosis inhibition impacted PAH pathobiology. Next, we determined how AAV1-mediated overexpression of the pro-ferroptotic protein acyl-CoA synthetase long-chain family member 4 (ACSL4)[15] in PAECs *in vivo* modulated pulmonary vascular disease burden to test the hypothesis that a pro-ferroptotic genetic intervention is sufficient to induce PAH. To gain mechanistic insights and probe potential cell-cell communication via released DAMPs, we defined how ferroptotic PAECs modulated PASMC and monocyte biology *in vitro*. Finally, we performed a human genetics association study to potentially link single nucleotide polymorphisms in ferroptosis genes with PH severity.

Methods

Data Availability Statement: Data sets, analysis, and study materials will be made available upon request to other researchers for the purpose of the results or replicating the procedures. All data of OMIC experiments are publicly available. The RNA-sequencing (RNA-seq) data are available at the NCBI Gene Expression Omnibus with the accession numbers GSE277179 and GSE277180. The mass spectrometry (MS) proteomics data are available at Figshare: DOI:10.6084/m9.figshare.27078124

Rodent Studies: Small-molecule mediated ferroptosis inhibition in the monocrotaline (MCT, Sigma-Aldrich) rat PAH model was evaluated in male Sprague-Dawley (Charles River) rats. Rodents were randomly assigned (coin flip by lead investigator) to one of three groups: 1. Control rats injected with phosphate buffered saline (*n*=5), 2. Rats injected with 60 mg/kg MCT and then treated with daily intraperitoneal injections of vehicle (2% dimethyl sulfoxide, 50% polyethylene glycol, 5% Tween 80, and 43% double distilled water) starting two weeks after MCT injection (*n*=10), and 3. MCT rats treated with daily intraperitoneal ferrostatin-1 (1 mg/kg, Selleck Chemicals) starting two weeks after MCT injection (*n*=10). End-point analysis was performed 24 days post MCT injection with primary physiological read-outs being right ventricular systolic pressure (RVSP) and effective arterial elastance (Ea). AAV1-GFP and AAV1-*Acsl4* at a dose of 0.3×10^{11} vector genomes were delivered via intratrachael injection the same day as low dose MCT (30 mg/kg). The end-point studies for viral study were conducted 24 days post treatment. Females were not evaluated due to the more robust phenotype observed in males. Sample size was estimated at *n*=10 based on previous experience with phenotypic variation and statistical power[16]. For AAV treatments, interim analysis was performed after *n*=5 rodents per group, and statistical differences in RVSP and Ea were observed so the study was terminated. No rodents were excluded. All rodent studies were approved by the University of Minnesota Institutional Animal Care and Use Committee

Cardiovascular Phenotyping: Echocardiography and closed-chest pressure-volume loop analyses quantified RV function and pulmonary vascular disease as we have previously described[16,17].

RNAsequencing: RNA from rat lung tissue was isolated from *n*=4 control, *n*=4 MCT-Vehicle and *n*=4 MCT-Fer-1 using PureLink RNA Mini kit (ThermoFisher) with DNase. RNA sequencing and library preparations were

conducted at the University of Minnesota Genomics Center via Illumina NovaSeq 6000 with 20 million reads per sample. PASMC cells were lysed and RNA was isolated using Purelink RNA Mini Kit (Invitrogen) according to kit instructions. RNA was submitted to University of Minnesota Genomics Center for library creation (TruSeq Stranded mRNA, converted to Aviti compatible with Element Adept Rapid PCR + kit) and >250×10^6 reads were generated.

Lung Mitochondrial Proteomics Analysis: Mitochondrial enrichments (Abcam) from lung tissue were performed according to manufactures instructions and were subjected to TMT16-plex (ThermoFisher Scientific) labeling and quantitative proteomics using Proteome Discover Software as previously described[16,17]. The lung mitochondrial-enriched proteome in *n*=5 control, *n*=5 MCT-Vehicle, and *n*=6 MCT-Fer-1 animals were analyzed.

Lung Metabolomics/Lipidomics: Global metabolomics analysis of frozen lung specimens on *n*=5 Control, *n*=5 MCT-Vehicle, and *n*=5 MCT-Fer-1 was performed at the University of Minnesota Center for Metabolomics and Proteomics using the Biocrates' MxP® Quant 500 kit. Samples were homogenized in a 2.0 mL Precelly standard tubes. Samples were centrifuged at 10,000*g* for 5 minutes at 4°C and supernatant was collected. 10µL of the extract was loaded and classes of metabolites were determined using 50µL of 1:1:1:0.16 water:EtOH:pyridine:phenyl isothiocyanate solution and incubated for an hour. ABSciex QTRAP 5500 triple-quadrupole (Farmington, MA, USA) mass spectrometer was used to perform the metabolomic assays.

Statistical Analysis: Statistical analyses were performed using Prism 9.0 (GraphPad Software). Normality of data was determined using the Shapiro-Wilk test. If data were normally distributed and there was equal variance as determined using the Brown-Forsythe test, 1-way analysis of variance with Tukey's multiple-comparisons test was performed. If there was unequal variance, Brown-Forsythe and Welch analysis of variance with Dunnett multiple-comparisons test was completed. If the data were not normally distributed, the Kruskal-Wallis test and Dunn's multiple-comparisons test were used when comparing two groups and the Mann Whitney U test for comparing two groups. Graphs display the mean or median value and all individual values. *p*-values of <0.05 were considered to indicate statistical significance. Hierarchical cluster analyses, sparse least discriminate analysis, random forest classification, and correlational heatmapping were performed using MetaboAnalyst software (https://www.metaboanalyst.ca/). The relative abundance of each protein was

determined using Proteome Discover Software. Transcripts and proteins that were significantly correlated ($p<0.05$) with right ventricular systolic pressure and end-arterial elastance (Ea) were processed for Kyoto Encyclopedia of Genes and Genomes (KEGG) using ShinyGO 0.76.3 (http://bioinformatics.sdstate.edu/go/).

For detailed Materials and Methods, please refer to the Online Supplement.

Results

Ferroptosis Inhibition Mitigated Pulmonary Vascular Remodeling and Improved Right Ventricular Function in Monocrotaline Rats

We first evaluated the physiological effects of ferroptosis in monocrotaline (MCT) rats using a translational approach by starting treatment two weeks after MCT injection. Ferrostatin-1 (1 mg/kg) imparted important therapeutic effects as it increased pulmonary artery acceleration time, reduced right ventricular systolic pressure (RVSP) and effective arterial elastance (Ea), and suppressed small pulmonary arterial remodeling (**Figure 1A-D**). Accordingly, right ventricular (RV) function as defined by Ees/Ea, tricuspid annular plane systolic excursion (TAPSE), and RV free wall thickening were all improved with ferrostatin-1 (**Figure 1E-G**). The summation of these data showed ferroptosis inhibition combatted pulmonary vascular remodeling and augmented RV function.

RNA-Sequencing and Lung Mitochondrial Proteomics Analyses Identified Links Between Ferroptosis and Pulmonary Hypertension Severity

Next, we used RNA-sequencing (RNA-seq) and quantitative proteomics analyses of lung samples to perform an unbiased assessment of pathways that were dysregulated as PAH severity increased. RNA-seq data revealed ferroptosis was the second most enriched pathway associated with higher Ea (**Figure 2A**). Correlational heatmapping identified multiple positive and significant associations between ferroptotic transcripts and Ea (**Figure 2B and C**). When evaluating pathways induced by higher RVSP, ferroptosis was not identified in our unbiased assessment (**Supplemental Figure 1**). However, correlational heatmapping again identified multiple ferroptotic transcripts were positively associated with RVSP (**Supplemental Figure 1**).

In our proteomics analysis, multiple metabolic pathways including the tricyclic acid cycle, fatty acid metabolism, oxidative phosphorylation, and amino acid metabolism were dysregulated as PAH severity increased. In agreement with our transcriptomic data, the ferroptosis pathway was enriched with increasing Ea and RVSP (**Figure 2 D and G**). Correlational heatmapping identified relationships between multiple ferroptotic proteins and Ea and RVSP (**Figure 2 E and H**). In particular, there were positive correlations between the pro-ferroptotic proteins, voltage-dependent anion-selective channel proteins 2 and 3 (VDAC 2/3), heme oxygenase

1 (HMOX1), and acyl-CoA synthetase long chain family members 1 and 5 (ACSL1/5) and Ea and RVSP (**Figure 2 F and I**). Conversely, the anti-ferroptotic protein poly(rC)-binding protein 2 (PCBP2) was negatively associated with Ea and RVSP (**Figure 2 F and I)**.

Ferrostatin-1 Restructured the Lung Lipidomic Signature

Because our proteomics analysis identified several metabolic pathways were associated with pulmonary hypertension severity, we performed a metabolomics/lipidomics analysis of whole lung extracts. Visual examination of hierarchical cluster analysis and sparse least squares discriminate analysis demonstrated differences in the overall metabolomics/lipidomic signature when the three experimental groups were compared (**Supplemental Figure 2A and B**). Random forest classification identified the 15 metabolites that differentiated the three groups, which were predominantly lipid species and the amino acid, glycine (**Supplemental Figure 2C**). We subsequently used hierarchical cluster analysis to evaluate ferrostatin-1's effects on three major lipid classes: phosphatidylcholines and lysophosphatidylcholines (PC, LPC), phosphatidylethanolamine and lysophosphatidylethanolamine (PE, LPE), and phosphatidylserine and lysophosphatidylserine (PS and LPS) as these lipids had the most significant differences when the three groups were compared. The most dramatic effects of ferrostatin-1 were on PC and LPC and PE and LPE. Ferrostatin-1 increased multiple PC and LPC species but reduced nearly all PE and LPE (**Supplemental Figure 2 D and E**). The effects of ferrostatin-1 on PS/LPS were less robust (**Supplemental Figure 2F**). When profiling amino acids, we found all amino acids other than glycine were elevated in MCT-Veh lungs when compared to controls, which was mostly mirrored in the ferrostatin-1 treatment animals with the exception of valine (**Supplemental Figure 2G**). Thus, ferroptosis inhibition appeared to have the greatest effect on lung lipid metabolism.

Ferroptosis Inhibition Suppressed Classical Complement Activation and Cytokine Signaling

Next, we probed our ferroptosis-complement hypothesis by interrogating the coagulation/complement pathway using RNA-seq, proteomics, and immunofluorescence approaches. Hierarchical cluster analysis of

RNA-seq data revealed ferrostatin-1 treatment blunted the upregulation of several coagulation/complement transcripts (**Figure 3A**). Correlational heatmapping displayed significant associations between multiple complement transcripts and RVSP and Ea (**Figure 3 B-E**). In particular, the transcript abundance of C1QA and C1QB were both correlated with Ea and RVSP (**Figure 3 C and E**). When this pathway was evaluated in our proteomic data, we also found ferroptosis inhibition prevented the upregulation of multiple complement proteins (**Figure 3F**). Correlational heatmapping again revealed several classical complement pathway proteins were associated with RVSP and Ea (**Figure 3 G-J**). To understand how ferrostatin-1 modulated complement activation in the pulmonary vasculature specifically, we used confocal microscopy to visualize perivascular complement deposition. In agreement with our proteomics and transcriptomics data, perivascular complement accumulation in MCT-Veh lungs was significantly elevated as compared to controls, but this response was mitigated by ferrostatin-1 (MCT-Veh: 1.8±0.2 fold increase compared to control, MCT-Fer-1: 1.1±0.2 fold increase compared to control p=0.02) (**Figure 3 K and L**).

Because complement promotes cytokine and chemokine release, we evaluated how ferrostatin-1 impacted the lung inflammatory/cytokine signaling pathway in our RNA-seq data. Hierarchical cluster analysis showed ferrostatin-1 reduced the abundance of multiple transcripts in the inflammatory/cytokine pathway as compared to MCT-Veh (**Supplemental Figure 3A)** In particular, ferrostatin-1 reduced transcript abundance of nodal growth differentiation factor (NODAL), a secreted ligand of the transforming growth factor-beta superfamily of proteins, the transcript that exhibited the strongest relationship with Ea (**Supplemental Figure 3B**). In addition, ferrostatin-1 lowered transcript levels of tumor necrosis factor receptor superfamily member 11a (TNFRSF11A), a member of the tumor necrosis factor family whose transcript levels were associated with PAH severity (**Supplemental Figure 3B**). Finally, levels of pro-inflammatory chemokines including C-X-C motif chemokine ligands (CXCL) 6/10 and C-C motif chemokine ligands (CCL) 9/21 were reduced with ferrostatin-1 (**Supplemental Figure 3B**). Importantly, CXCL10 and CCL21 levels were positively associated with Ea (**Supplemental Figure 3C**).

Deconvolution RNA-seq Analysis Revealed Ferrostatin-1 Modulated Endothelial Cell, Smooth Muscle Cell, Interstitial Macrophage Abundance and Metabolic and Inflammatory Phenotypes

To define how ferrostatin-1 modulated the cellular landscape of the pulmonary vasculature, we performed deconvolution RNA-seq analysis to define the changes in cell populations and pathways that were impacted by ferroptosis inhibition. All three experimental groups exhibited distinct cellular compositions in the lungs, but heterogeneity was observed (**Figure 4A, Supplemental Table 1**). Correlational heatmapping identified relationships between the proportion of cell types in the samples and Ea and RVSP (**Figure 4B and C**). Cell types known to underlie PAH pathobiology including smooth muscle cells, endothelial cells, and interstitial macrophages were most strongly associated with Ea and RVSP. Smooth muscle cells had the most robust correlational relationship with RVSP and Ea (**Figure 4D**). Importantly, ferrostatin-1 treatment partially mitigated the increase in lung smooth muscle cells when compared to MCT-Veh rats (**Figure 4D**). Additionally, ferroptosis inhibition partially suppressed the reduction of endothelial cells in the EA1 population and the increase in EA2 population. However, the reduction in EA1 as opposed to the increase in EA2 cells (data not shown) was more significantly associated with PAH severity (**Figure 4E and F**). Additionally, greater abundance of interstitial macrophages was associated with more severe PAH as MCT-Veh rats had the highest numbers of interstitial macrophages (**Figure 4 E and F**). Ferroptosis inhibition lowered interstitial macrophage numbers as compared to MCT-Veh (**Figure 4 E and F**). Pathway analysis delineated how ferrostatin-1 modulated the transcriptional environment in highly abundant cells. Ferroptosis inhibition suppressed the activation of multiple pathways in both endothelial cells and macrophages. In both cell types, changes in the DNA damage, cellular replication (PI3K/AKT/mTOR signaling and mitotic spindle), heme metabolism, and lipid handling (adipogenesis) pathways were observed (**Figure 4G**). Finally, we used confocal microscopy to evaluate how ferroptosis modulated macrophage infiltration into the pulmonary vasculature. There was a significant increase in perivascular $CD11b^+$ cells in the MCT-Veh animals as compared to control animals, which ferrostatin-1 treatment reduced (MCT-Veh: 10.4±0.9 $CD11b^+$ cells/arteriole, MCT-Fer-1: 4.3±0.5 $CD11b^+$ cells/arteriole $p=2.5\times10^{-5}$) (**Figure 4H**).

Ferroptotic Media from Human Pulmonary Artery Endothelial Cells Promoted Pathogenic Changes in Human Pulmonary Artery Smooth Muscle Cells and Human Monocytes

To supplement our multi-omics analysis and provide more mechanistic data using human cells, we next determined how media from ferroptotic human PAEC, which contained ferroptotic DAMPs, impacted *in vitro*

phenotypes of human PASMC and human monocytes. Incubating PASMC with ferroptotic PAEC DAMPs (**Figure 5A**) altered the transcriptomic landscape as there were 699 differentially expressed genes when PASMC treated with ferroptotic media were compared to PASMC treated with control media. Hierarchical cluster analysis demonstrated the two conditions resulted in distinct RNA signatures (**Figure 5B**). Pathway analysis of transcripts upregulated by ferroptotic media suggested there were alterations in metabolic pathways including amino acid metabolism, hypoxia inducible factor-1 (HIF1), and mammalian target of rapamycin (mTOR) signaling (**Figure 5C**). Pathway analysis of the downregulated transcripts identified an enrichment of pathways important for regulation DNA integrity/repair and cell cycle regulation (**Figure 5C**). Next, we used confocal microscopy as a cellular readout of our RNA-seq results. Ferroptotic media disrupted the mitochondrial network as characterized by increased fragmentation and a reduced mitochondrial footprint (**Figure 5D**). Because PASMC DNA repair and cell cycle regulation gene programs were altered by ferroptotic PAEC DAMPs, we evaluated PASMC proliferation status because DNA damage is associated with PASMC replication in PAH[18]. Ferroptotic DAMPs heightened PASMC proliferation as the proportion of $Ki67^{+}$ cells was significantly higher than control media (Control Media:40±5%, Ferroptotic Media: 67±6%, p=0.03) (**Figure 5E**)

Then, we used flow cytometry to probe how PAEC ferroptotic DAMPs altered monocyte inflammatory status *in vitro* (**Figure 5F and G**). We first found ferroptotic media promoted monocyte survival (**Figure 5H**). Moreover, ferroptotic media induced a pro-inflammatory signature, as there were significantly increased proportions of cells that expressed high levels of the pro-inflammatory markers CD86 (Control Media: 14±1%, Ferroptotic Media: 34±5%, p=0.005), CD209 (Control Media: 11±0.4%, Ferroptotic Media: 37±0.3%, $p=5.1\times10^{-8}$), a significantly lower proportion of cells that expressed the anti-inflammatory and pro-efferocytic marker MerTK (Control Media: 80±1%, Ferroptotic Media: 69±1%, p=0.0005), and a nonsignificant increase in the proportion of cells expressing high levels of CD80 (**Figure 5G-K**). These data suggested ferroptotic PAEC DAMPs stimulated survival and a pro-inflammatory phenotype in human monocytes.

Viral-Mediated Endothelial Cell Overexpression of the Pro-Ferroptotic Protein ACSL4 Induced an Inflammatory Pulmonary Hypertension Phenotype

Next, we used a genetic approach to complement our small-molecule data to evaluate the role of ferroptosis in rodent pulmonary hypertension by comparing the effects of intratracheal delivery of AAV1-*Acsl4* (*n*=5) or AAV1-GFP (*n*=5), driven by the endothelial cell specific cadherin-5[19] promoter, in rats exposed to low dose (30 mg/kg) monocrotaline (**Figure 6A**). Immunofluorescence analysis demonstrated heightened ACSL4 immunoreactivity in endothelial cell layer adjacent to PASMC in the AAV1-*Acls4* treated rats as compared to AAV1-GFP rats (**Figure 6A**). Physiological characterization revealed AAV1-*Acsl4* induced moderate pulmonary hypertension with significantly reduced pulmonary artery acceleration time (AAV1-GFP: 19±1 ms, AAV1-*Acsl4*: 15±1 ms, *p*=0.02) (**Figure 6B**) and elevated RVSP (AAV1-GFP: 33±2 mmHg, AAV1-*Acsl4*: 55±3 mm Hg, *p*=0.0004) (**Figure 6C**) and Ea (AAV1-GFP: 0.1±0.02 mmHg/μL, AAV1-*Acsl4*: 0.3±0.05 mmHg/μL, *p*=0.0004) (**Figure 6D**). Unfortunately, one of the AAV1-*Acsl4* rats died during the hemodynamic study so only 4 animals had complete hemodynamic characterization. AAV1-*Acsl4* heightened pathological small vessel pulmonary vascular remodeling (**Figure 6E**) and peri-vascular complement deposition (**Figure 6F**). The alterations in the pulmonary vasculature induced right ventricular cardiomyocyte hypertrophy (**Figure 6G**) and compromised right ventricular function (**Figure 6 H-J**). In conclusion, these data demonstrated genetically-initiated PAEC ferroptosis via ACSL4 overexpression induced an inflammatory pulmonary hypertension.

Presence of Single-Nucleotide Polymorphisms in Ferroptosis Genes Potentially Associated with More Severe Pulmonary Hypertension

Finally, we evaluated how the presence of single-nucleotide polymorphisms (SNPs) in ferroptosis genes impacted noninvasive and invasive measures of pulmonary hypertension in a mixed cohort of patients evaluated at the Vanderbilt BioVU biorepository. The presence of six SNPs in ferroptosis genes, which were characterized as variants of unknown significance with four SNPs resulting in amino acid substitutions and two SNPs were located in intronic sequences, were associated with more severe pulmonary hypertension using both echocardiographic and hemodynamic measures, however the overall frequency was low (**Supplemental Table 2**). Therefore, we pooled all six SNPs and compared how carriers of ferroptosis SNPs compared to those lacking potentially pathogenic SNPs. In an unadjusted analysis, carriers had significantly higher RVSP [Carriers: 63.9 (45.0-80.6), Noncarriers: 46.8 mmHg (35.0-62.0), *p*=0.0001] as determined by

echocardiography (**Figure 7A**). Furthermore, invasively measured mean pulmonary arterial pressure (mPAP) [Carriers: 40.0 (25.0-51.0), Noncarriers: 31.0 mmHg (22.0-41.0), p=0.02], and pulmonary vascular resistance (PVR) [Carriers: 4.3 (2.4-6.9), Noncarriers: 2.6 Wood units (1.7-4.6), p=0.001] were higher in those harboring ferroptosis SNPs (**Figure 7 B-C**). Because this was a mixed cohort, we performed a multivariate regression analysis and even after correcting for age, race, sex, presence of heart failure, chronic obstructive pulmonary disease, and use of pulmonary vasodilators, ferroptotic SNPs were independently associated with higher RVSP, mPAP, and PVR (**Figure 7 D-E**). These data highlight a potential link between ferroptosis and pulmonary hypertension severity in humans. However, future studies are needed to determine how these SNPs regulate proteins function or alter splicing to provide further understanding of how these SNPs may impact ferroptotic regulation.

Discussion

In summary, our translational rodent studies show small molecule inhibition of ferroptosis mitigates PAH and improves right ventricular function in MCT rats even when implemented after PAH has developed. Transcriptomics and proteomics analyses demonstrate a relationship between ferroptosis induction and PAH severity, which provides unbiased data to support our physiological findings. Our metabolomics/lipidomics experiments suggest ferrostatin-1 most robustly modulates lung lipid metabolism. In the pulmonary vasculature, suppression of ferroptosis alters endothelial and pulmonary artery smooth muscle cell numbers and gene activation patterns. Additionally, ferrostatin-1 mitigates pathological immune activation in the lung by suppressing perivascular complement deposition, lowering cytokines and chemokines, and reducing interstitial macrophage abundance. *In vitro* studies support our deconvolution RNA-seq experimental results as media containing DAMPs from ferroptotic PAEC promotes pathogenic changes in human PASMC marked by alterations in metabolic pathways including HIF/mTOR signaling and pathways responsible for DNA homeostasis. These transcriptomic changes are paired with mitochondrial morphological alterations and heightened proliferation rates. In addition, ferroptotic PAEC DAMPs induce a pro-inflammatory phenotype in human monocytes. Furthermore, we provide genetic evidence that PAEC ferroptosis is sufficient to induce pulmonary hypertension as AAV1-*Acsl4* results in an inflammatory pulmonary hypertension with associated right ventricular dysfunction in rats. Finally, a human genetic-association study reveals SNPs in ferroptosis genes are potentially associated with more severe pulmonary vascular disease burden. In conclusion, our data support a model in which ferroptotic PAECs release DAMPs that promote ectopic complement activation, serve as a signal to recruit and activate pro-inflammatory macrophages to the pulmonary vasculature, and alter the transcriptomic landscape of PASMC in a manner that recapitulates PAH pathobiology. The summation of these cellular and molecular alterations ultimately promote pulmonary hypertension (**Central Figure**). However, future work targeting each of these steps *in vivo* is required to further refine our working model.

Our data suggest PAEC ferroptosis drives pulmonary hypertension by both altering the PASMC genetic program and activating inflammatory monocytes/macrophages. Incubation of PASMC with ferroptotic endothelial cell media modulates pathways already implicated in PAH pathobiology. First, we show ferroptotic PAECs reduces PASMC DNA repair pathway transcript abundances. DNA damage triggers PASMC proliferation and dysfunction as there is increased DNA damage in PASMC in PAH[18]. Importantly, modulation

of DNA damage repair pathways counteracts pulmonary vascular remodeling and reduces pulmonary hypertension severity in rodents[18,20]. Moreover, transcriptomic data suggest ferroptotic PAEC media activates HIF1[21] and mTOR[22], two pathways with a wealth of data demonstrating their pathogenic roles in PAH. In addition, ferroptotic endothelial cell DAMPs increase monocyte survival and promote a pro-inflammatory phenotype *in vitro*, demonstrating another established link to PAH pathobiology. These data are in line with other manuscripts showing inhibition of ferroptosis suppresses inflammatory signaling via the NOD-, LRR-, and pyrin domain-containing protein 3 (NLRP3) inflammasome activation in the lung[6] and heightened levels of interstitial macrophage in human PAH lungs[13]. Certainly, future work is required to understand what specific components of the DAMPs released from ferroptotic PAECs drive the changes in PASMC and macrophages so more discrete and targetable approaches can be employed.

Our findings that ferroptosis induces both metabolic derangements and pathological inflammation in the lungs has potential to link two heavily implicated molecular phenotypes in PAH pathology to one targetable pathway. In PAH, derangements in lung metabolism including altered fatty acid oxidation[23,24], heightened anaerobic glucose metabolism[23], and disrupted amino acid utilization[25-27] are well documented. Ferroptosis has the potential to impact several catabolic pathways via its ability to suppress electron transport chain activity[28], a final common pathway for nearly all metabolic processes. While targeting specific metabolic arms including suppression of fatty acid oxidation[29] and activation of glucose oxidative metabolism[30] has robust therapeutic effects in preclinical PAH, the translation of these studies to humans has not been met with overwhelming success[31]. Perhaps, targeting one isolated branch of metabolism is insufficient to counteract human PAH pathogenesis, and more broad-based metabolic interventions would garner greater success. In addition, ferroptosis antagonism also combats ectopic complement activation, lowers levels of several cytokines/chemokines, and mitigates macrophage infiltration demonstrates the anti-inflammatory effects of ferrostatin-1 in the pulmonary vasculature. While there is strong data showing many individual cell types or cytokines/chemokines promote PAH in rodents[32]; unfortunately the translation of these findings to humans has not been as fruitful as desired. In particular, antagonism of interleukin-6 signaling with tocilizumab[33] or depletion of B-cells with rituximab[34] did not significantly change PAH severity in two small clinical trials. Perhaps suppressing an individual cytokine or immune cell type may not be the most effective therapy in humans as available data suggests there is widespread immune activation in PAH[32]. In fact, the cross-talk

between immune and pulmonary vascular cells is crucial for PAH progression/severity as there is greater immune-pulmonary vascular interactions in hereditary PAH as compared to idiopathic PAH, and this finding correlates with hemodynamic severity[35]. Because our data suggests ferroptosis both dampens mitochondrial metabolism and initiates innate immune system activation in the pulmonary vasculature, perhaps approaches to counteract ferroptosis may lead to greater translational success by combatting both metabolic and inflammatory mechanisms.

We show ferroptosis inhibition mitigates pulmonary hypertension severity in MCT rats and ferroptosis induction via AAV-*Acsl4* causes pulmonary hypertension. These results are congruent with additional preclinical and human data that support our hypothesis that ferroptosis promotes pulmonary hypertension. First, several ferroptosis-suppressing molecules exhibit therapeutic efficacy in relevant preclinical models of pulmonary vascular disease including MCT, Sugen-hypoxia, and chronic hypoxia rats and lambs with persistent pulmonary hypertension of the newborn (**Table 1**). In addition, KEGG and WIKI pathway analysis of upregulated transcripts in PAH endothelial cells analyzed by single cell RNA-seq[36] identifies ferroptosis as an enriched pathway in PAH (**Supplemental Figure 4**). Furthermore, a proteomic study demonstrates a 35% reduction in glutathione peroxidase-4, an anti-ferroptotic protein, in PAECs from PAH patients[37]. Moreover, there are higher systemic levels of lipid peroxidation in PAH patients as urinary abundance of isoprostaglandin F2a are significantly higher than controls[38]. Finally, circulating levels of transferrin receptor, a proposed biomarker of ferroptosis[39], are elevated in PAH patients and can independently predict mortality[40]. In addition, higher circulating levels of transferrin receptor levels are associated with more severe pulmonary hypertension in patients with chronic lung disease[41]. Thus the summation of our results, other published pre-clinical therapeutic evaluations, and human transcriptomics, proteomics, and biomarker data suggest ferroptosis may be a targetable pathway to suppress adverse pulmonary vascular remodeling.

In our proteomics analysis of the lungs, we highlighted multiple mitochondrial metabolic pathways which are altered as pulmonary hypertension severity increases. However, the metabolomics/lipidomics analysis suggested the greatest effect of ferrostatin-1 was on lipid metabolism. In particular, ferrostatin-1 increases levels of multiple phosphatidylcholines (**Supplemental Figure 2**), which may have direct relevance to mitochondrial function because phosphatidylcholines are a major component of the mitochondrial membrane system[42]. Perhaps the greater concentrations of phosphatidylcholines contributes to the proteomic changes in

other metabolic pathways via the stabilization and preservation of mitochondria. In addition, phosphatidylcholines are required for inner membrane protein translocases in the mitochondria[42]. A change in phosphatidylcholines could also alter mitochondrial protein stability as matrix and inner membrane proteins may not be properly trafficked into the mitochondria in the PAH lung due to the dysregulation of phosphatidylcholines. Additionally, ferrostatin-1 lowered the levels of nearly all phosphatidylethanolamines profiled (**Supplemental Figure 2**). This may be an important feedback mechanism to mitigate ferroptosis because peroxidation of phosphatidylethanolamines is crucial for ferroptosis initiation[43]. Surprisingly, ferrostatin-1 had almost no effect on lung amino acid abundances with the exception of reducing levels of valine, a branched chain amino acid. While amino acids regulate ferroptosis homeostasis in other conditions[44], our data suggest amino acids may not play a dominant role in endothelial cell ferroptosis induction in PAH. In conclusion, the strongest effects of ferrostatin-1 on lung metabolism appears to be on lipid homeostasis, and these changes may underlie some of the beneficial physiological effects of ferroptosis antagonism.

Our deconvolution RNA-seq analysis identifies changes in pulmonary endothelial cell, smooth muscle cell, and interstitial macrophage number and gene activation patterns. However, other immune cell types undoubtedly contribute to pulmonary vascular remodeling, but our approach may have not been sensitive enough to detect changes in these lower abundant immune cell populations. Certainly, there is literature demonstrating T-cells[45,46] and B-cells[47] play important roles in pulmonary vascular remodeling, however we did not observe changes in these cell populations with ferroptosis inhibition (**Supplemental Table 1**). In addition, we did not see a profound alteration in mast cell numbers with ferrostatin-1 treatment (**Supplemental Table 1**). With the limitations of our approach, it appears ferroptosis inhibition exerted the greatest effects on endothelial cells, smooth muscle cells, and recruited macrophages. The complex interplay between these distinct cell types in the pulmonary vasculature appears to be responsible for adverse effects of ferroptosis in pathological pulmonary vascular remodeling (**Central Figure**).

Limitations

Our work has important limitations that we must acknowledge. First, we used whole lung tissue in our proteomics and metabolomics analyses, and unfortunately defining what cell types are contributing to the

observed changes cannot be determined. We tried to overcome some of these limitations by using deconvolution RNA-seq to nominate changes in cell numbers and gene activation patterns and by performing *in vitro* analyses of the most altered cell types: monocytes and PASMC. Finally, our SNP analysis was conducted in a mixed population of pulmonary hypertension patients in a small cohort. When we evaluated these SNPs in a larger secondary cohort: the UK PAH Cohort study[43], we found they were in very low abundance and not associated with differences in PAH severity in an unadjusted analysis (**Supplemental Figure 5**). Finally, we evaluated phenotypes only in males because of the more robust phenotype in male rodents.

Acknowledgements

We thank the Center for Metabolomics and Proteomics and the Genomics Center at the University of Minnesota for providing services related to the generation of RNAseq and proteomics data.

Disclosures

KWP received grant funding from Bayer unrelated to this manuscript.

Sources of Funding

SZP is funded by an American Heart Association Career Development Award (23CDA1049093, https://doi.org/10.58275/AHA.23CDA1049093.pc.gr.167948) and by NIH K08 HL168166. ELB is funded by NIH R01s FD007627, HL146588, HL163960, HL155278, DK124845, and NIH R61 HL158941. This work was supported by the NIHR BioResource which supports the UK National Cohort of Idiopathic and Heritable PAH; the British Heart Foundation (BHF SP/12/12/29836) and the UK Medical Research Council (MR/K020919/1). CJR is supported by BHF Basic Science Research fellowship (FS/SBSRF/21/31025). JWW is funded by NIH R01s HL166843 and AI165553. KWP is funded by NIH R01s HL158795 and HL162927. The Orbitrap Eclipse instrumentation platform used in this work was purchased through High-end Instrumentation Grant S10OD028717 from the NIH.

Figure 1: Ferrostatin-1 Treatment Combatted Pulmonary Hypertension Severity and Improved Right Ventricular Function in Monocrotaline Rats. (A) Ferrostatin-1 (1 mg/kg) treatment increased pulmonary artery acceleration time in MCT rats [Con: 26±1 (*n*=5), MCT-Veh: 16±1 (*n*=10), MCT-Fer-1: 21±1 ms (*n*=10)]. (B) Ferroptosis inhibition with ferrostatin-1 reduced right ventricular systolic pressure (RVSP) (Con: 21±1, MCT-Veh: 69±7, MCT-Fer-1: 46±2 mmHg), *p*-values determined by Kruskal-Wallis test. (C) Effective arterial elastance (E_a) was lowered by ferroptosis inhibition (Con: 0.08±0.02, MCT-Veh: 0.40±0.04, MCT-Fer-1: 0.25±0.02 mmHg/μL), *p*-values determined by Kruskal-Wallis test. (D) Small vessel pulmonary arterial remodeling was blunted by ferrostatin-1 (Median values averaged from 4 animals per group: Con: 26±1, MCT-Veh: 43±3 MCT-Fer-1: 28±3, *p*-values determined by ANOVA with Tukey's multiple comparisons test]. (E) Ferrostatin-1 treatment improved right ventricular-pulmonary artery coupling (E_{es}/E_a) (Con: 1.3±0.2, MCT-Veh: 0.37±0.04, MCT-Fer-1: 0.88±0.08), *p*-values determined by Brown-Forsythe and Welch ANOVA test), TAPSE (Con: 2.3±0.1, MCT-Veh: 1.7±0.05, MCT-Fer-1: 2.2±0.1, *p*-values determined by Kruskal-Wallis test) (F) and RV free wall thickening (Con: 84±8, MCT-Veh: 26±5, MCT-Fer-1: 67±5, *p*-values determined by ANOVA with Tukey's multiple comparisons test) (G).

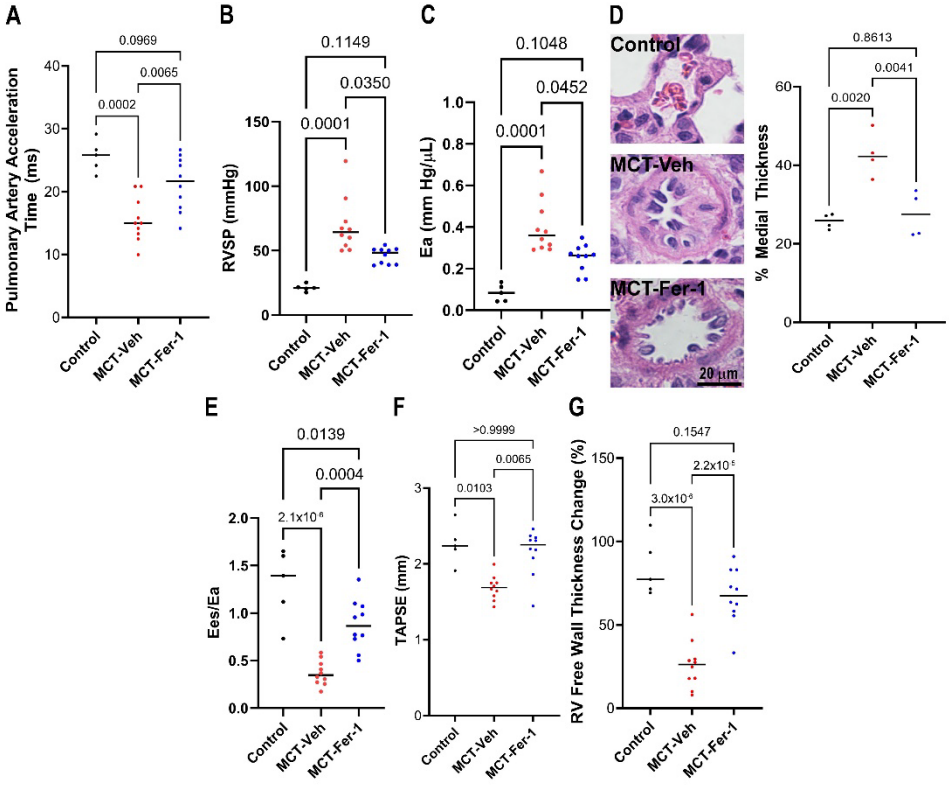
A
Pulmonary Artery Acceleration Time (ms)
0.0969
0.0065
0.0002
Control
MCT-Veh
MCT-Fer-1
B
RVSP (mmHg)
0.1149
0.0350
0.0001
C
Ea (mm Hg/μL)
0.1048
0.0452
0.0001
D
Control
MCT-Veh
MCT-Fer-1
20 μm
% Medial Thickness
0.8613
0.0041
0.0020
E
Ees/Ea
0.0139
0.0004
2.1x10⁻⁶
F
TAPSE (mm)
>0.9999
0.0065
0.0103
G
RV Free Wall Thickness Change (%)
0.1547
2.2x10⁻⁵
3.0x10⁻⁶

Figure 2: Lung RNA-sequencing and Proteomics Analyses Identified Associations Between Ferroptosis and Pulmonary Hypertension Severity. (A) Pathway analysis of transcripts isolated from whole lung specimens from (*n*=4 control, *n*=4 MCT-Veh, and *n*=3 MCT-Fer-1) significantly associated with Ea. (B) Correlational heat mapping of ferroptosis pathway transcripts and Ea. (C) Ten transcripts most strongly associated with Ea. (D) Pathway analysis of proteins (*n*=5 control, *n*=5 MCT-Veh, and *n*=6 MCT-Fer-1 animals) significantly associated with Ea. (E) Correlational heat map of ferroptosis proteins with Ea. (F) Ferroptosis proteins most strongly associated with Ea. (G) Pathway analysis of proteins significantly associated with right ventricular systolic pressure (RVSP). (H) Correlational heat map of ferroptosis proteins and RVSP. (I) Ten most strongly associated ferroptosis proteins with RVSP.

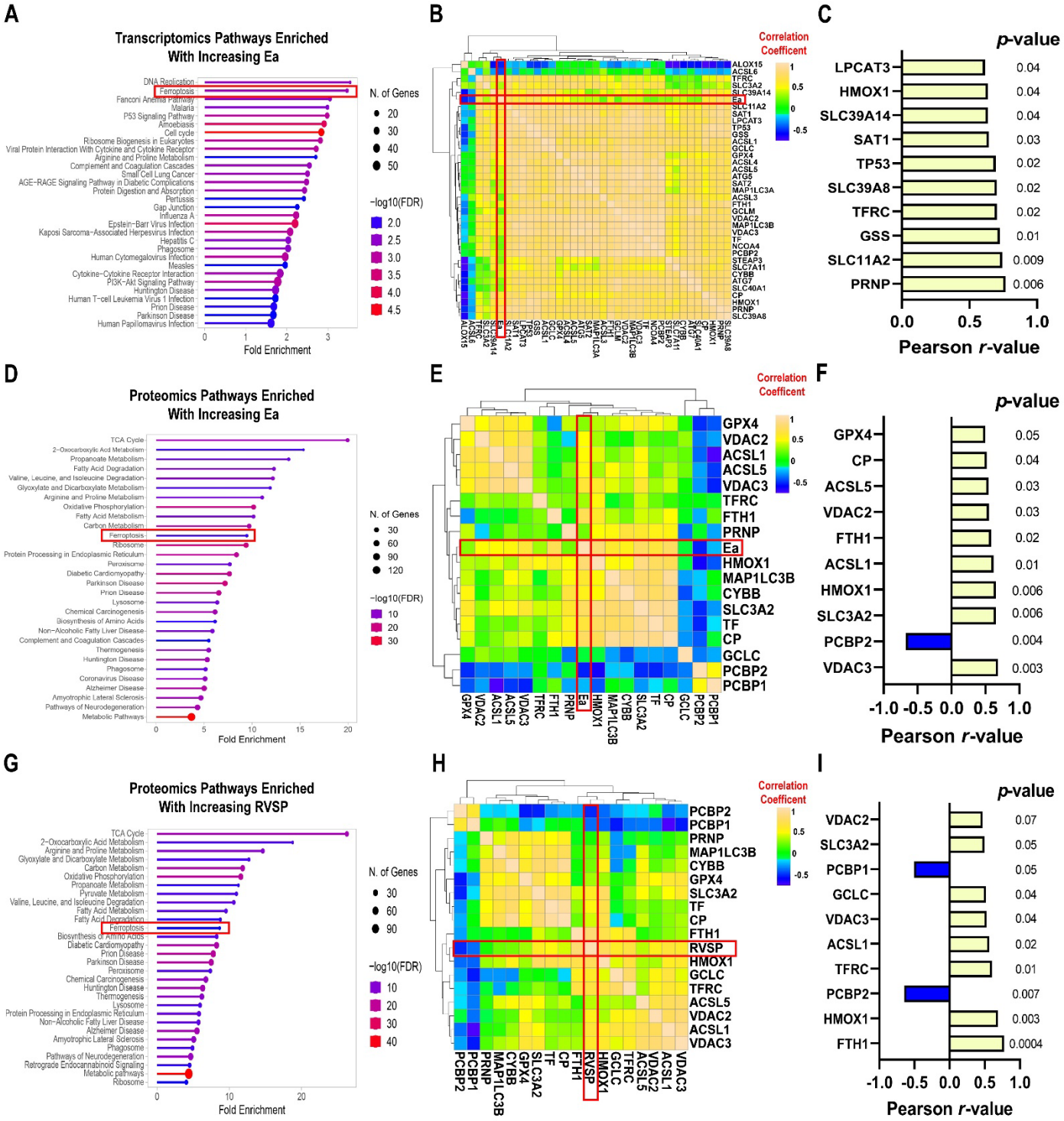
A
Transcriptomics Pathways Enriched With Increasing Ea
DNA Replication
Ferroptosis
Fanconi Anemia Pathway
Malaria
P53 Signaling Pathway
Amoebiasis
Cell cycle
Ribosome Biogenesis in Eukaryotes
Viral Protein Interaction With Cytokine and Cytokine Receptor
Arginine and Proline Metabolism
Complement and Coagulation Cascades
Small Cell Lung Cancer
AGE-RAGE Signaling Pathway in Diabetic Complications
Protein Digestion and Absorption
Pertussis
Gap Junction
Influenza A
Epstein-Barr Virus Infection
Kaposi Sarcoma-Associated Herpesvirus Infection
Hepatitis C
Phagosome
Human Cytomegalovirus Infection
Measles
Cytokine-Cytokine Receptor Interaction
PI3K-Akt Signaling Pathway
Huntington Disease
Human T-cell Leukemia Virus 1 Infection
Prion Disease
Parkinson Disease
Human Papillomavirus Infection
0 1 2 3
Fold Enrichment
N. of Genes
20
30
40
50
-log10(FDR)
2.0
2.5
3.0
3.5
4.0
4.5
B
Correlation Coefficent
1
0.5
0
-0.5
ALOX15
ACSL6
TFRC
SLC3A2
SLC39A14
Ea
SLC11A2
SAT1
LPCAT3
TP53
GSS
ACSL1
GCLC
GPX4
ACSL4
ACSL5
ATG5
SAT2
MAP1LC3A
ACSL3
FTH1
GCLM
VDAC2
MAP1LC3B
VDAC3
TF
NCOA4
PCBP2
STEAP3
SLC7A11
CYBB
ATG7
SLC40A1
CP
HMOX1
PRNP
SLC39A8
C
p-value
LPCAT3 0.04
HMOX1 0.04
SLC39A14 0.04
SAT1 0.03
TP53 0.02
SLC39A8 0.02
TFRC 0.02
GSS 0.01
SLC11A2 0.009
PRNP 0.006
0.0 0.5 1.0
Pearson r-value
D
Proteomics Pathways Enriched With Increasing Ea
TCA Cycle
2-Oxocarboxylic Acid Metabolism
Propanoate Metabolism
Fatty Acid Degradation
Valine, Leucine, and Isoleucine Degradation
Glyoxylate and Dicarboxylate Metabolism
Arginine and Proline Metabolism
Oxidative Phosphorylation
Fatty Acid Metabolism
Carbon Metabolism
Ferroptosis
Ribosome
Protein Processing in Endoplasmic Reticulum
Peroxisome
Diabetic Cardiomyopathy
Parkinson Disease
Prion Disease
Lysosome
Chemical Carcinogenesis
Biosynthesis of Amino Acids
Non-Alcoholic Fatty Liver Disease
Complement and Coagulation Cascades
Thermogenesis
Huntington Disease
Phagosome
Coronavirus Disease
Alzheimer Disease
Amyotrophic Lateral Sclerosis
Pathways of Neurodegeneration
Metabolic Pathways
0 5 10 15 20
Fold Enrichment
N. of Genes
30
60
90
120
-log10(FDR)
10
20
30
E
Correlation Coefficent
1
0.5
0
-0.5
GPX4
VDAC2
ACSL1
ACSL5
VDAC3
TFRC
FTH1
PRNP
Ea
HMOX1
MAP1LC3B
CYBB
SLC3A2
TF
CP
GCLC
PCBP2
PCBP1
F
p-value
GPX4 0.05
CP 0.04
ACSL5 0.03
VDAC2 0.03
FTH1 0.02
ACSL1 0.01
HMOX1 0.006
SLC3A2 0.006
PCBP2 0.004
VDAC3 0.003
-1.0 -0.5 0.0 0.5 1.0
Pearson r-value
G
Proteomics Pathways Enriched With Increasing RVSP
TCA Cycle
2-Oxocarboxylic Acid Metabolism
Arginine and Proline Metabolism
Glyoxylate and Dicarboxylate Metabolism
Carbon Metabolism
Oxidative Phosphorylation
Propanoate Metabolism
Pyruvate Metabolism
Valine, Leucine, and Isoleucine Degradation
Fatty Acid Metabolism
Fatty Acid Degradation
Ferroptosis
Biosynthesis of Amino Acids
Diabetic Cardiomyopathy
Prion Disease
Parkinson Disease
Peroxisome
Chemical Carcinogenesis
Huntington Disease
Thermogenesis
Lysosome
Protein Processing in Endoplasmic Reticulum
Non-Alcoholic Fatty Liver Disease
Alzheimer Disease
Amyotrophic Lateral Sclerosis
Phagosome
Pathways of Neurodegeneration
Retrograde Endocannabinoid Signaling
Metabolic pathways
Ribosome
0 10 20
Fold Enrichment
N. of Genes
30
60
90
-log10(FDR)
10
20
30
40
H
Correlation Coefficent
1
0.5
0
-0.5
PCBP2
PCBP1
PRNP
MAP1LC3B
CYBB
GPX4
SLC3A2
TF
CP
FTH1
RVSP
HMOX1
GCLC
TFRC
ACSL5
VDAC2
ACSL1
VDAC3
I
p-value
VDAC2 0.07
SLC3A2 0.05
PCBP1 0.05
GCLC 0.04
VDAC3 0.04
ACSL1 0.02
TFRC 0.01
PCBP2 0.007
HMOX1 0.003
FTH1 0.0004
-1.0 -0.5 0.0 0.5 1.0
Pearson r-value

Figure 3: Ferroptosis Inhibition Mitigated Ectopic Complement Activation in the Lungs of MCT Rats (A) Hierarchical cluster analysis of transcripts in the complement coagulation pathway. (A) Ferrostatin-1 reduced levels of many transcripts as compared to MCT-Veh. (B) Correlational heat map of complement/coagulation transcripts with Ea. (C) Identification of 10 transcripts most strongly associated with Ea. Classical complement components C1Qa and C1Qb were higher as Ea increased. (D) Correlational heat map of complement/coagulation transcripts with RVSP. (E) Ten transcripts most strongly associated with RVSP. (F) Hierarchical cluster analysis of proteins in the complement/coagulation cascade. (G) Correlational heat map of complement/coagulation proteins with Ea. (H) Identification of 10 proteins most strongly associated with Ea. (I) Correlational heat map of complement/coagulation proteins with RVSP. (J) Identification of 10 proteins most strongly associated with RVSP. (K) Representative confocal micrographs showed increased complement deposition around the pulmonary vasculature in MCT-Vehicle, which was mitigated by ferrostatin-1. (L) Quantification of perivascular C3 intensity. *p*-values determined by Kruskal-Wallis test and Dunn's multiple comparisons test.

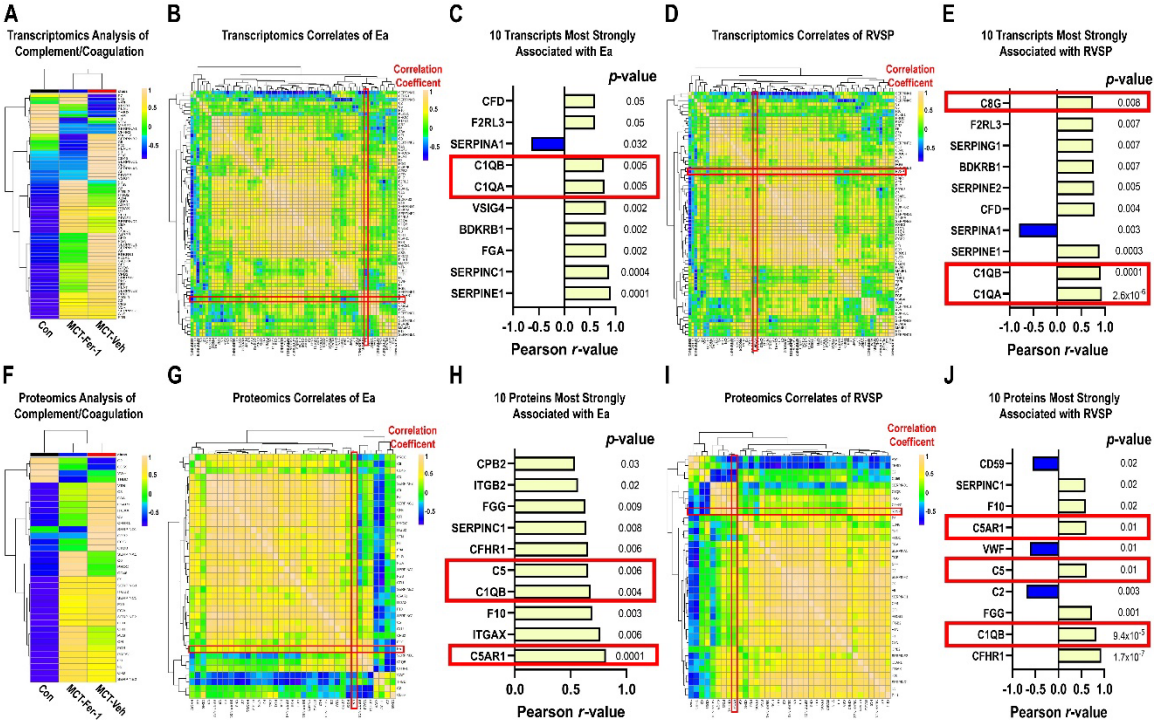
A
Transcriptomics Analysis of Complement/Coagulation
Con
MCT-Fer-1
MCT-Veh
B
Transcriptomics Correlates of Ea
Correlation Coefficent
C
10 Transcripts Most Strongly Associated with Ea
p-value
CFD 0.05
F2RL3 0.05
SERPINA1 0.032
C1QB 0.005
C1QA 0.005
VSIG4 0.002
BDKRB1 0.002
FGA 0.002
SERPINC1 0.0004
SERPINE1 0.0001
-1.0 -0.5 0.0 0.5 1.0
Pearson r-value
D
Transcriptomics Correlates of RVSP
Correlation Coefficent
E
10 Transcripts Most Strongly Associated with RVSP
p-value
C8G 0.008
F2RL3 0.007
SERPING1 0.007
BDKRB1 0.007
SERPINE2 0.005
CFD 0.004
SERPINA1 0.003
SERPINE1 0.0003
C1QB 0.0001
C1QA 2.6x10-6
-1.0 -0.5 0.0 0.5 1.0
Pearson r-value
F
Proteomics Analysis of Complement/Coagulation
Con
MCT-Fer-1
MCT-Veh
G
Proteomics Correlates of Ea
Correlation Coefficent
H
10 Proteins Most Strongly Associated with Ea
p-value
CPB2 0.03
ITGB2 0.02
FGG 0.009
SERPINC1 0.008
CFHR1 0.006
C5 0.006
C1QB 0.004
F10 0.003
ITGAX 0.006
C5AR1 0.0001
0.0 0.5 1.0
Pearson r-value
I
Proteomics Correlates of RVSP
Correlation Coefficent
J
10 Proteins Most Strongly Associated with RVSP
p-value
CD59 0.02
SERPINC1 0.02
F10 0.02
C5AR1 0.01
VWF 0.01
C5 0.01
C2 0.003
FGG 0.001
C1QB 9.4x10-5
CFHR1 1.7x10-7
-1.0 -0.5 0.0 0.5 1.0
Pearson r-value

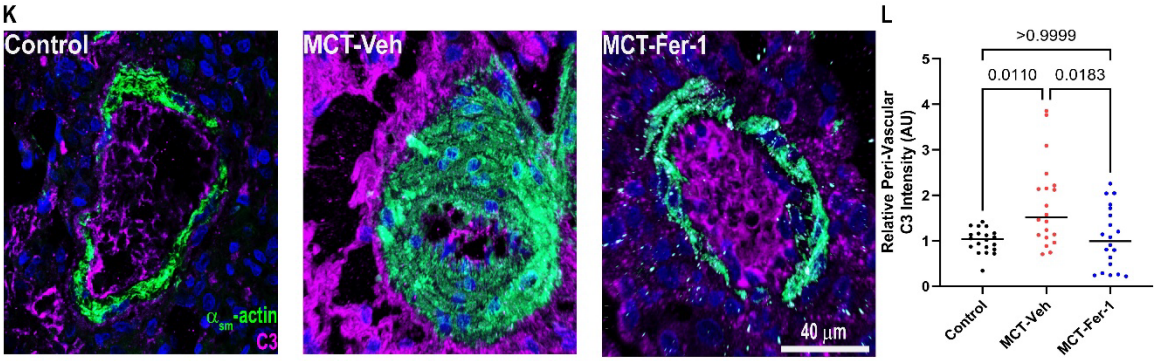
K
Control
MCT-Veh
MCT-Fer-1
αsm-actin
C3
40 µm
L
>0.9999
0.0110
0.0183
Relative Peri-Vascular C3 Intensity (AU)
0
1
2
3
4
5
Control
MCT-Veh
MCT-Fer-1

Figure 4: Deconvolution RNA-sequencing Demonstrated Ferroptosis Inhibition Modulated Endothelial, Smooth Muscle, and Interstitial Macrophage Abundances and Gene Activation Patterns. (A) Map of cell type abundances in control, MCT-Veh, and MCT-Fer-1 animals as determined by deconvolution RNA-seq (*n*=4 control, *n*=4 MCT-Veh, and *n*=4 MCT-Fer-1). Correlational heat mapping identified relationships between cell type abundances and Ea (B) and RVSP (C). (D) Relationships between smooth muscle cell abundance and Ea and RVSP. (E) Relationships between endothelial cell population 1 (EA1) and Ea and RVSP. (F) Relationships between interstitial macrophage population and Ea and RVSP. (G) Pathway analysis of transcriptomic changes in endothelial cells, macrophages, and total cells with ferrostatin-1 treatment. (H) Representative images of pulmonary arteriole demonstrating perivascular $CD11b^+$ positive cells (arrow) and quantification of peri-vascular $CD11b^+$ cells. *p*-values determined by Kruskal-Wallis test and Dunn's multiple comparisons test.

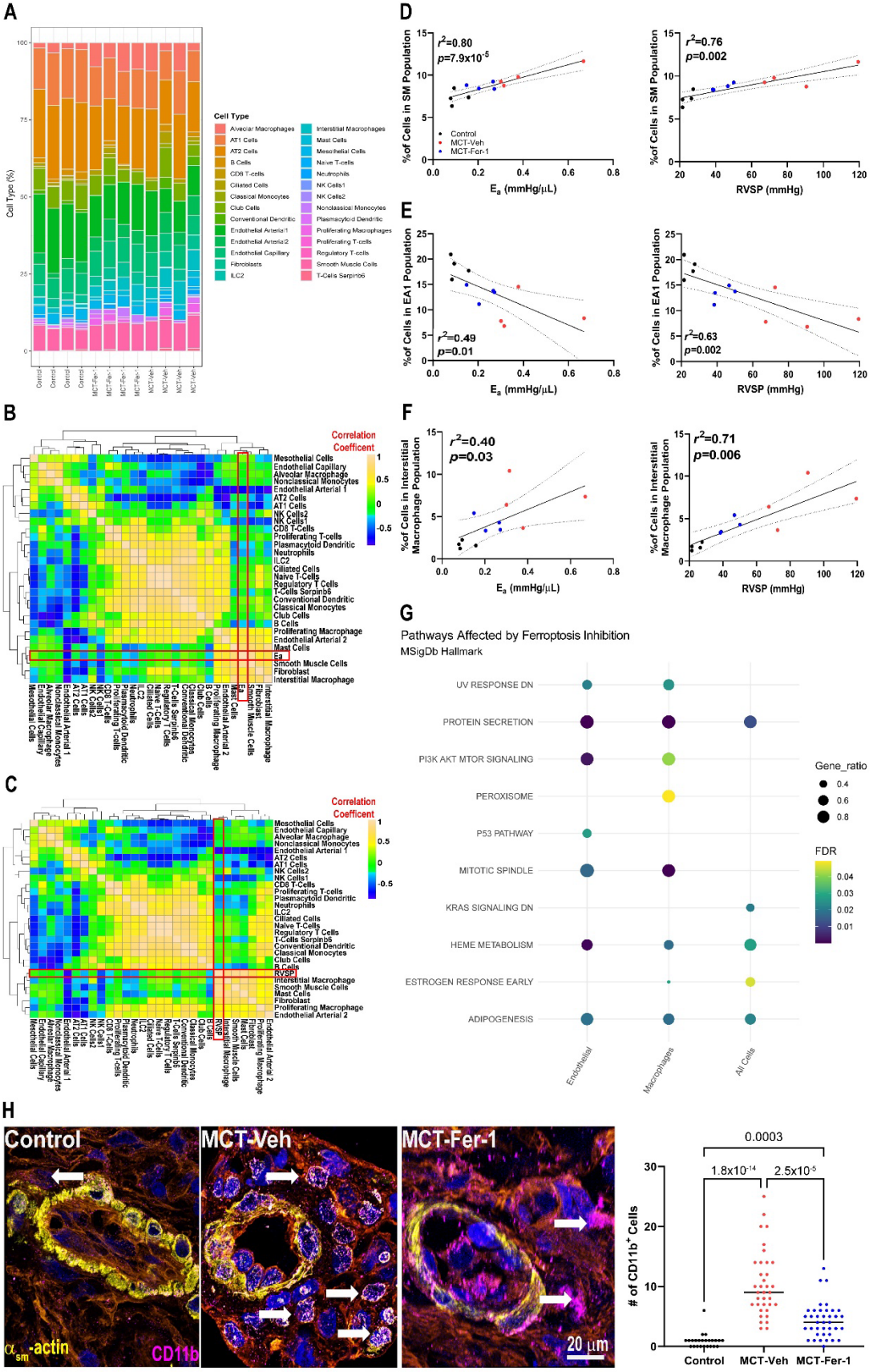
A
Cell Type (%)
Cell Type
Alveolar Macrophages
AT1 Cells
AT2 Cells
B Cells
CD8 T-cells
Ciliated Cells
Classical Monocytes
Club Cells
Conventional Dendritic
Endothelial Arterial1
Endothelial Arterial2
Endothelial Capillary
Fibroblasts
ILC2
Interstitial Macrophages
Mast Cells
Mesothelial Cells
Naive T-cells
Neutrophils
NK Cells1
NK Cells2
Nonclassical Monocytes
Plasmacytoid Dendritic
Proliferating Macrophages
Proliferating T-cells
Regulatory T-cells
Smooth Muscle Cells
T-Cells Serpinb6
B
Correlation Coefficent
C
Correlation Coefficent
D
r^2=0.80
p=7.9x10^{-5}
Control
MCT-Veh
MCT-Fer-1
%of Cells in SM Population
E_a (mmHg/μL)
r^2=0.76
p=0.002
RVSP (mmHg)
E
r^2=0.49
p=0.01
%of Cells in EA1 Population
r^2=0.63
p=0.002
F
r^2=0.40
p=0.03
%of Cells in Interstitial Macrophage Population
r^2=0.71
p=0.006
G
Pathways Affected by Ferroptosis Inhibition
MSigDb Hallmark
UV RESPONSE DN
PROTEIN SECRETION
PI3K AKT MTOR SIGNALING
PEROXISOME
P53 PATHWAY
MITOTIC SPINDLE
KRAS SIGNALING DN
HEME METABOLISM
ESTROGEN RESPONSE EARLY
ADIPOGENESIS
Endothelial
Macrophages
All Cells
Gene_ratio
FDR
H
Control
MCT-Veh
MCT-Fer-1
α_{sm}-actin
CD11b
20 μm
0.0003
1.8x10^{-14}
2.5x10^{-5}
# of CD11b$^+$ Cells

Figure 5: DAMPs from Ferroptotic Human Pulmonary Arterial Endothelial Cells Recapitulated Pathogenic Changes in Human Pulmonary Artery Smooth Muscle Cells and Promoted a Pro-Inflammatory Phenotype in Human Monocytes *In Vitro*. (A) Diagram of experimental approach to evaluate the effects of ferroptotic pulmonary artery endothelial cells on pulmonary artery smooth muscle cell phenotypes *in vitro*. (B) Hierarchical cluster analysis of top 699 transcripts from RNA isolated from *n*=4 replicates of PASMC treated with control media and *n*=4 replicates of PASMC treated with ferroptotic media. (C) KEGG pathway analysis of upregulated and downregulated transcripts comparing control and ferroptotic media treated PASMC. (D) Super resolution confocal micrographs of PASMC incubated with control and ferroptotic PAEC spent media stained with MitoTracker Orange and DAPI and quantification of the mitochondrial footprint. *p*-value determined by Mann Whitney test. (E) Confocal micrographs of PASMC stained with DAPI and Ki67 to identify replicating cells. Red arrows indicate Ki67^{+} cells, white arrows indicate Ki67^{-} cells. Quantification of the proportion of Ki67^{+} cells, *p*-value determined by Mann Whitney test. (F) Diagram of experimental conditions employed to evaluate *in vitro* effects of ferroptotic PAECs on isolated human monocytes. (G) Quantification of the number of viable monocytes following media exposure. *p*-value determined by unpaired *t*-test. Flow cytometry analysis of monocyte expression of CD86 (H), CD209 (H), MerTK (J), and CD80 (K). *p*-values determined by unpaired *t*-test in H, I, and J and unpaired *t*-test with Welch correction in K.

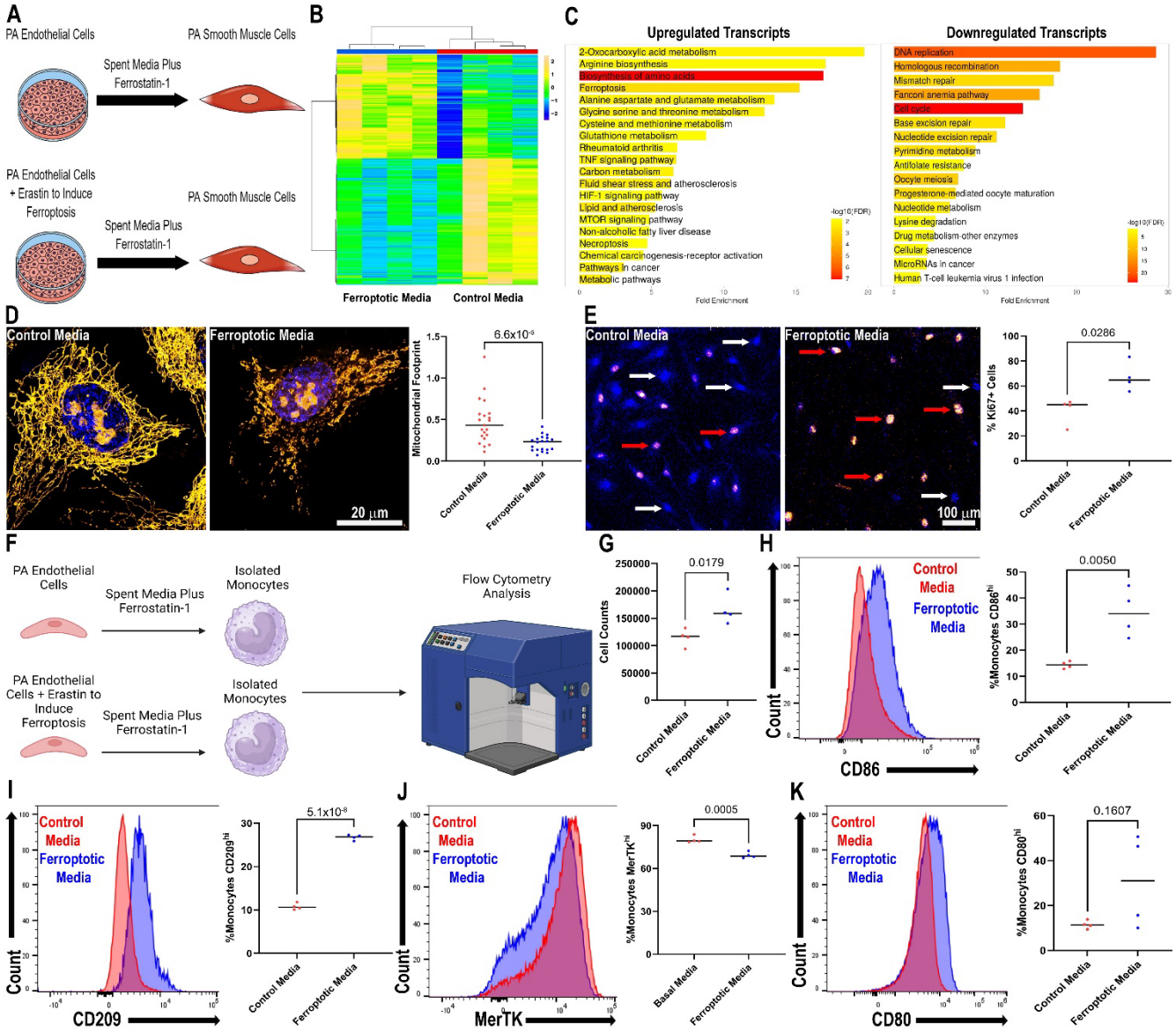
A
PA Endothelial Cells
PA Smooth Muscle Cells
Spent Media Plus Ferrostatin-1
PA Endothelial Cells + Erastin to Induce Ferroptosis
PA Smooth Muscle Cells
Spent Media Plus Ferrostatin-1
B
Ferroptotic Media
Control Media
C
Upregulated Transcripts
2-Oxocarboxylic acid metabolism
Arginine biosynthesis
Biosynthesis of amino acids
Ferroptosis
Alanine aspartate and glutamate metabolism
Glycine serine and threonine metabolism
Cysteine and methionine metabolism
Glutathione metabolism
Rheumatoid arthritis
TNF signaling pathway
Carbon metabolism
Fluid shear stress and atherosclerosis
HIF-1 signaling pathway
Lipid and atherosclerosis
MTOR signaling pathway
Non-alcoholic fatty liver disease
Necroptosis
Chemical carcinogenesis-receptor activation
Pathways in cancer
Metabolic pathways
-log10(FDR)
Fold Enrichment
Downregulated Transcripts
DNA replication
Homologous recombination
Mismatch repair
Fanconi anemia pathway
Cell cycle
Base excision repair
Nucleotide excision repair
Pyrimidine metabolism
Antifolate resistance
Oocyte meiosis
Progesterone-mediated oocyte maturation
Nucleotide metabolism
Lysine degradation
Drug metabolism-other enzymes
Cellular senescence
MicroRNAs in cancer
Human T-cell leukemia virus 1 infection
-log10(FDR)
Fold Enrichment
D
Control Media
Ferroptotic Media
20 μm
6.6x10-5
Mitochondrial Footprint
Control Media
Ferroptotic Media
E
Control Media
Ferroptotic Media
100 μm
0.0286
% Ki67+ Cells
Control Media
Ferroptotic Media
F
PA Endothelial Cells
Spent Media Plus Ferrostatin-1
Isolated Monocytes
PA Endothelial Cells + Erastin to Induce Ferroptosis
Spent Media Plus Ferrostatin-1
Isolated Monocytes
Flow Cytometry Analysis
G
0.0179
Cell Counts
Control Media
Ferroptotic Media
H
Control Media
Ferroptotic Media
Count
CD86
0.0050
%Monocytes CD86hi
Control Media
Ferroptotic Media
I
Control Media
Ferroptotic Media
Count
CD209
5.1x10-8
%Monocytes CD209hi
Control Media
Ferroptotic Media
J
Control Media
Ferroptotic Media
Count
MerTK
0.0005
%Monocytes MerTKhi
Basal Media
Ferroptotic Media
K
Control Media
Ferroptotic Media
Count
CD80
0.1607
%Monocytes CD80hi
Control Media
Ferroptotic Media

Figure 6: AAV1-Mediated Endothelial *ACSL4* Overexpression Induced Perivascular Complement Deposition, Pulmonary Hypertension, and Right Ventricular Dysfunction in Rats. (A) Schematic presentation of experimental approach of rats treated with $0.3x10^{11}$ vector genomes of AAV1-*Acsl4* or $0.3x10^{11}$ vector genomes of AAV1-GFP with concurrent exposure to low dose (30 mg/kg) monocrotaline with confocal micrographs demonstrating heightened ACSL4 immunoreactivity in the endothelial cell layer (arrows). AAV1-*Acsl4* treatment induced pulmonary hypertension as pulmonary artery acceleration time was reduced [AAV1-GFP: 19±1 ms (*n*=5) AAV1-*Acsl4*: 15±0.7 ms (*n*=5)] (B) and RVSP [AAV1-GFP: 33±2 mm Hg (*n*=5), AAV1-*Acsl4*: 55±3 mm Hg (*n*=4)] (C), Ea [AAV1-GFP: 0.12±0.2 (*n*=5), AAV1-*Acsl4*: 0.29±0.05 (*n*=4)] (D) were increased and small vessel remodeling was heightened (E). (F) Representative confocal micrographs and quantification of C3 immunofluorescence intensity demonstrated AAV1-*Acsl4* promoted perivascular complement deposition. AAV1-*Acsl4* induced RV cardiomyocyte hypertrophy (AAV1-GFP: 364±5 μm^2, AAV1-*Acsl4*: 407±5 μm^2) (G) and RV dysfunction as RV-PA coupling was compromised [AAV1-GFP: 1.4±0.1 (*n*=5), AAV1-*Acsl4*: 0.6±0.1 (*n*=4)] (H) and cardiac output [AAV1-GFP: 140±12 mL/min (*n*=5) (I), AAV1-*Acsl4*: 99±11 mL/min (*n*=5)] and RV free wall thickening [AAV1-GFP: 75±9% (*n*=5), AAV1-*Acsl4*: 38±8% (*n*=5)] were impaired (J). *p*-values as determined by unpaired t-test (B, C, H, and I) or Mann-Whitney test (D-G, and J)

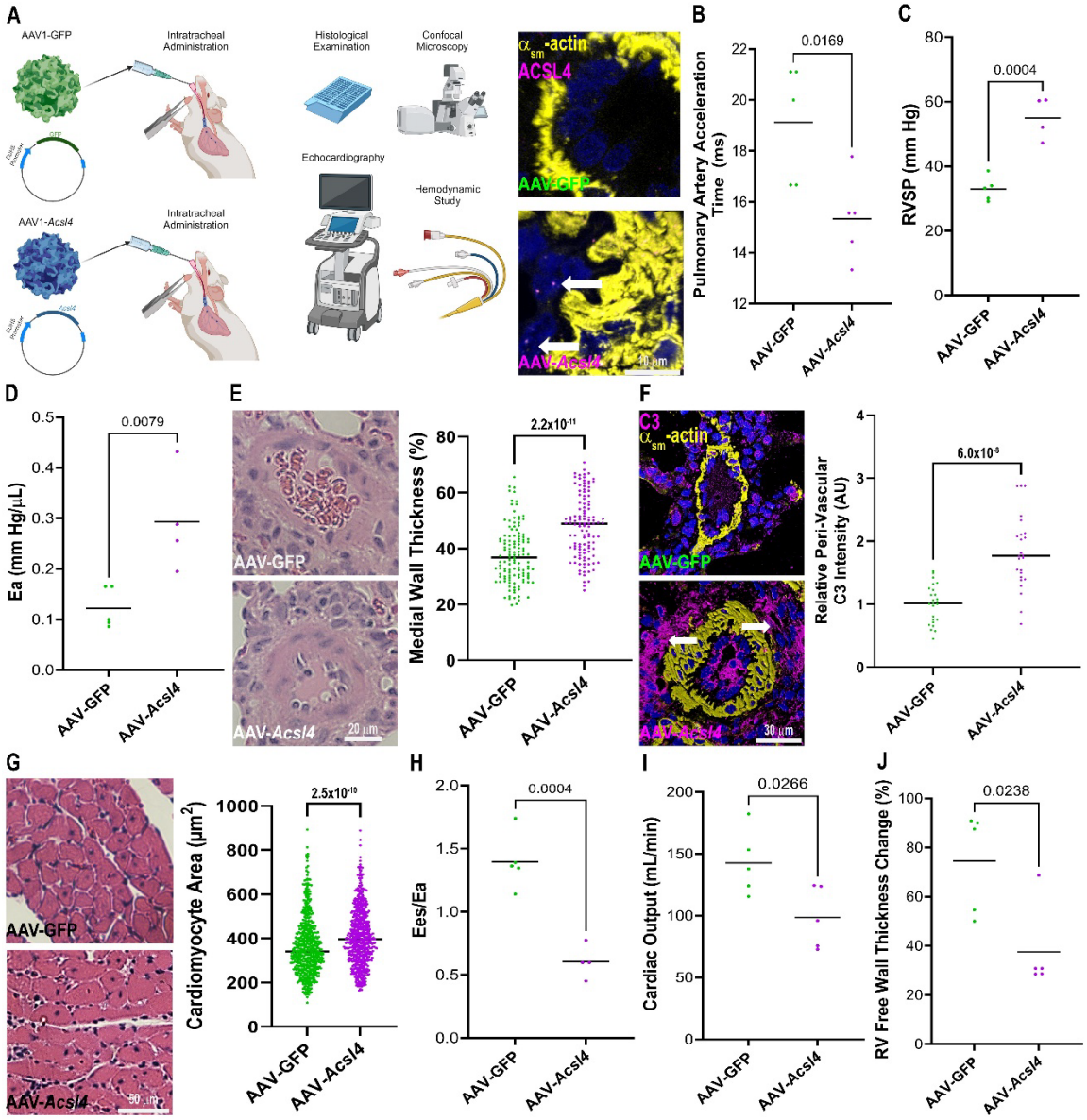
A
AAV1-GFP
Intratracheal Administration
Histological Examination
Confocal Microscopy
Echocardiography
Hemodynamic Study
AAV1-Acsl4
Intratracheal Administration
αsm-actin
ACSL4
AAV-GFP
AAV-Acsl4
20 µm
B
0.0169
Pulmonary Artery Acceleration Time (ms)
AAV-GFP
AAV-Acsl4
C
0.0004
RVSP (mm Hg)
AAV-GFP
AAV-Acsl4
D
0.0079
Ea (mm Hg/µL)
AAV-GFP
AAV-Acsl4
E
AAV-GFP
AAV-Acsl4
20 µm
2.2x10-11
Medial Wall Thickness (%)
AAV-GFP
AAV-Acsl4
F
C3
αsm-actin
AAV-GFP
AAV-Acsl4
30 µm
6.0x10-8
Relative Peri-Vascular C3 Intensity (AU)
AAV-GFP
AAV-Acsl4
G
AAV-GFP
AAV-Acsl4
50 µm
2.5x10-10
Cardiomyocyte Area (µm2)
AAV-GFP
AAV-Acsl4
H
0.0004
Ees/Ea
AAV-GFP
AAV-Acsl4
I
0.0266
Cardiac Output (mL/min)
AAV-GFP
AAV-Acsl4
J
0.0238
RV Free Wall Thickness Change (%)
AAV-GFP
AAV-Acsl4

Figure 7: Presence of Single Nucleotide Polymorphisms in Ferroptosis Regulating Genes Was Associated With More Severe Pulmonary Hypertension. (A) Patients harboring SNPs in ferroptosis genes had higher right ventricular systolic pressures [Carriers: 63.9 (45.0-80.6), Noncarriers 46.8 (35.0-62.0), median (25th-75th percentiles)] as determined by echocardiography, (B) invasively measured mean pulmonary arterial pressure [Carriers: 40.0 (25.0-51.0), Noncarriers 31.0 (22.0-41.0), median (25th-75th percentiles)], and pulmonary vascular resistance [Carriers: 4.3 (2.4-6.9), Noncarriers 2.6 (1.7-4.6), median (25th-75th percentiles)] as determined by invasive hemodynamic studies (C). *p*-values as determined by Mann-Whitney U-test. Forest plots depicted correlational co-efficient with standard errors and calculated *p*-values when RVSP (D), mPAP (E), and PVR (F) were modeled in multivariate regression analysis.

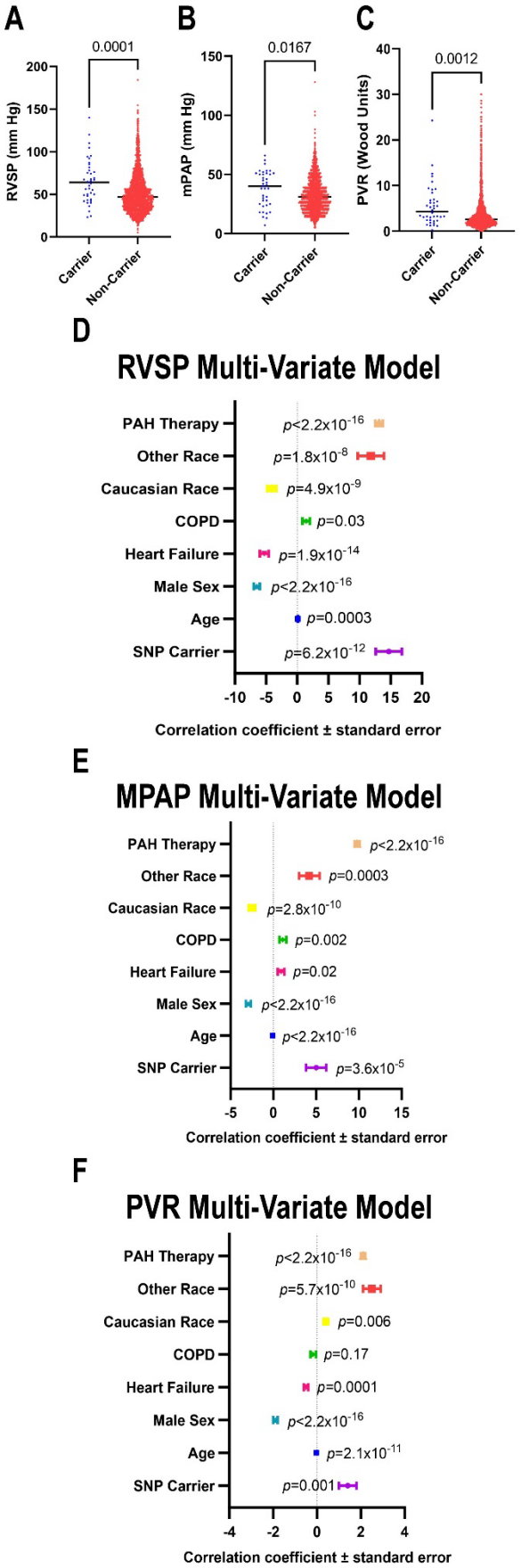
A
0.0001
RVSP (mm Hg)
200
150
100
50
0
Carrier
Non-Carrier
B
0.0167
mPAP (mm Hg)
150
100
50
0
Carrier
Non-Carrier
C
0.0012
PVR (Wood Units)
40
30
20
10
0
Carrier
Non-Carrier
D
RVSP Multi-Variate Model
PAH Therapy
Other Race
Caucasian Race
COPD
Heart Failure
Male Sex
Age
SNP Carrier
p<2.2x10-16
p=1.8x10-8
p=4.9x10-9
p=0.03
p=1.9x10-14
p<2.2x10-16
p=0.0003
p=6.2x10-12
-10 -5 0 5 10 15 20
Correlation coefficient ± standard error
E
MPAP Multi-Variate Model
PAH Therapy
Other Race
Caucasian Race
COPD
Heart Failure
Male Sex
Age
SNP Carrier
p<2.2x10-16
p=0.0003
p=2.8x10-10
p=0.002
p=0.02
p<2.2x10-16
p<2.2x10-16
p=3.6x10-5
-5 0 5 10 15
Correlation coefficient ± standard error
F
PVR Multi-Variate Model
PAH Therapy
Other Race
Caucasian Race
COPD
Heart Failure
Male Sex
Age
SNP Carrier
p<2.2x10-16
p=5.7x10-10
p=0.006
p=0.17
p=0.0001
p<2.2x10-16
p=2.1x10-11
p=0.001
-4 -2 0 2 4
Correlation coefficient ± standard error

Central Figure: Proposed Model for the Pathogenic Role of Endothelial Cell Ferroptosis in PAH Pathobiology

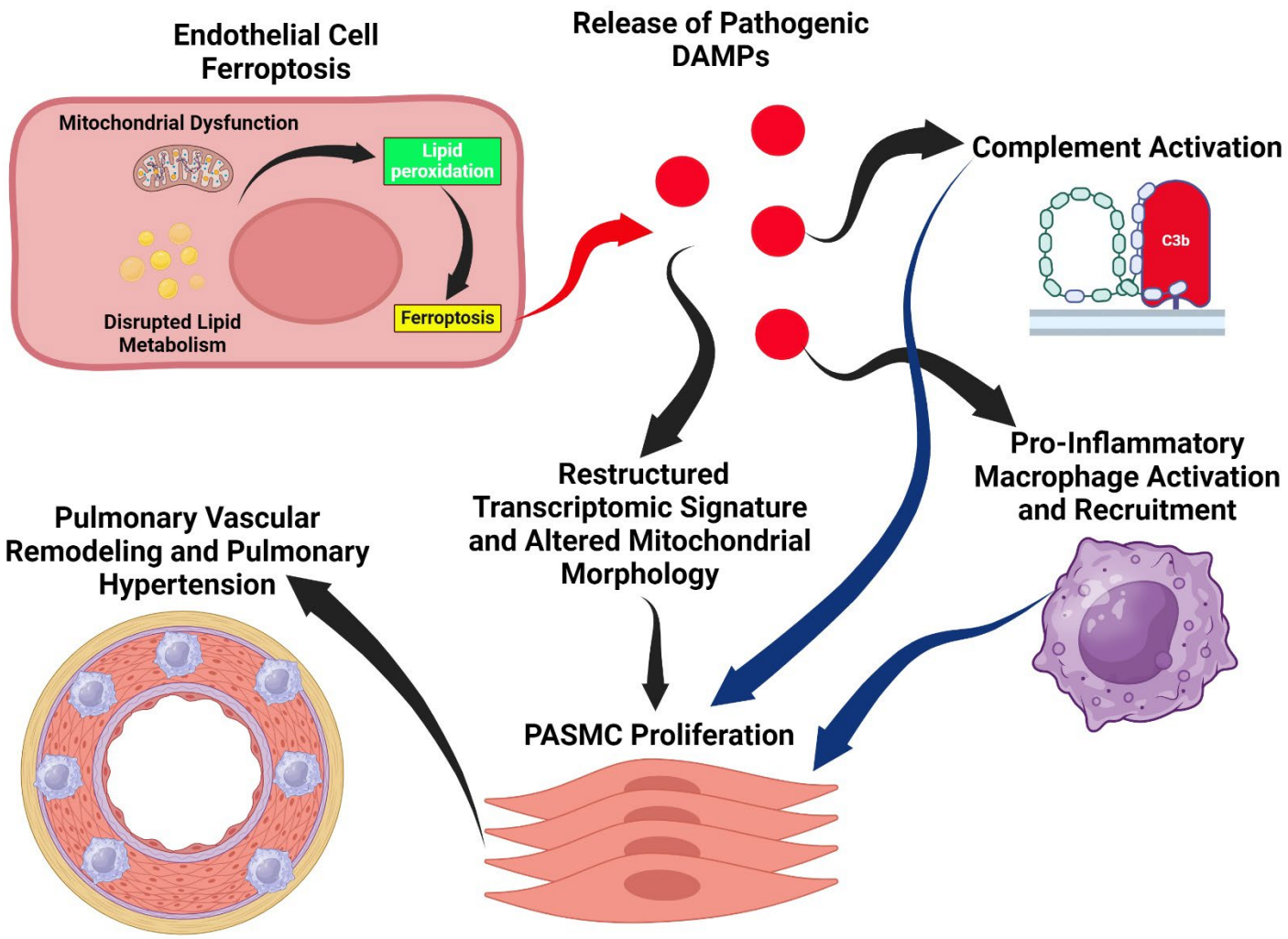

Table 1: Numerous Ferroptosis Suppressing Drugs Combat Pulmonary Hypertension in Multiple Preclinical Models

Small Molecules	Proposed Mechanisms of Ferroptosis Suppression	Animal Models With Therapeutic Effects
AICAR and metformin	AMPK Activation	Chronic hypoxia-induced pulmonary hypertension in rats, Sugen-hypoxia induced pulmonary hypertension, monocrotaline rats[48]
Apocyin	Reduces reactive oxygen species required for lipid peroxidation in the NOX family of proteins	Lambs with persistent pulmonary hypertension of the newborn[49]
Deferoxamine	Iron chelation to prevent iron-dependent lipid peroxidation	Chronic hypoxia-induced pulmonary hypertension in rats[50]
Ferrostatin-1	Suppresses ferroptosis directly and mitigates NLRP3 Activation in the lungs	Monocrotaline-induced pulmonary hypertension in rats[6,8]
MK866	Inhibits lipoxygenase-mediated lipid peroxidation	Chronic hypoxia-induced pulmonary hypertension in rats[51]
Rosiglitazone/pioglitazone	Antagonizes ACSL4-induced conversion of free fatty acids into fatty CoA esters that then become peroxidated	Monocrotaline rats, sugen-hypoxia rats, chronic hypoxia rats, $ApoE^{-/-}$ mice, transgenic TGFβ1 mice[52]
Rapamycin	mTOR Suppression	Monocrotaline-induced pulmonary hypertension in rats, chronic hypoxia-induced pulmonary hypertension in mice and rats, Sugen-hypoxia rats[53]
Vildagliptin	Blocks DPP4-mediated lipid peroxidation	Monocrotaline-induced pulmonary hypertension in rats, chronic hypoxia-induced pulmonary hypertension in rats[54]
Zileuton	Inhibits lipoxygenase-mediated lipid peroxidation	Monocrotaline pulmonary hypertension[55]

Abbreviations: AMPK: Adenosine monophosphate activate protein kinase, NOX: NADPH oxidases, ACSL4: acyl-CoA synthetase long-chain family member 4, mTOR: mammalian target of rapamycin, DPP4: dipeptidyl-dippeditase-4.

References

1. Stockwell BR. Ferroptosis turns 10: Emerging mechanisms, physiological functions, and therapeutic applications. *Cell*. 2022;185:2401-2421. doi: 10.1016/j.cell.2022.06.003
2. Dixon SJ, Lemberg KM, Lamprecht MR, Skouta R, Zaitsev EM, Gleason CE, Patel DN, Bauer AJ, Cantley AM, Yang WS, et al. Ferroptosis: an iron-dependent form of nonapoptotic cell death. *Cell*. 2012;149:1060-1072. doi: 10.1016/j.cell.2012.03.042
3. Friedmann Angeli JP, Schneider M, Proneth B, Tyurina YY, Tyurin VA, Hammond VJ, Herbach N, Aichler M, Walch A, Eggenhofer E, et al. Inactivation of the ferroptosis regulator Gpx4 triggers acute renal failure in mice. *Nat Cell Biol*. 2014;16:1180-1191. doi: 10.1038/ncb3064
4. Bai T, Li M, Liu Y, Qiao Z, Wang Z. Inhibition of ferroptosis alleviates atherosclerosis through attenuating lipid peroxidation and endothelial dysfunction in mouse aortic endothelial cell. *Free Radic Biol Med*. 2020;160:92-102. doi: 10.1016/j.freeradbiomed.2020.07.026
5. Culley MK, Chan SY. Mitochondrial metabolism in pulmonary hypertension: beyond mountains there are mountains. *J Clin Invest*. 2018;128:3704-3715. doi: 10.1172/JCI120847
6. Xie SS, Deng Y, Guo SL, Li JQ, Zhou YC, Liao J, Wu DD, Lan WF. Endothelial cell ferroptosis mediates monocrotaline-induced pulmonary hypertension in rats by modulating NLRP3 inflammasome activation. *Sci Rep*. 2022;12:3056. doi: 10.1038/s41598-022-06848-7
7. Liao J, Xie SS, Deng Y, Wu DD, Meng H, Lan WF, Dai P. PRDX6-mediated pulmonary artery endothelial cell ferroptosis contributes to monocrotaline-induced pulmonary hypertension. *Microvasc Res*. 2023;146:104471. doi: 10.1016/j.mvr.2022.104471
8. Song J, Chen Y, Wang S, Dong Z, Liu X, Li X, Zhang Z, Sun L, Zhong J. Ferrostatin-1 Blunts Right Ventricular Hypertrophy and Dysfunction in Pulmonary Arterial Hypertension by Suppressing the HMOX1/GSH Signaling. *J Cardiovasc Transl Res*. 2024;17:183-196. doi: 10.1007/s12265-023-10423-4
9. Sun Y, Chen P, Zhai B, Zhang M, Xiang Y, Fang J, Xu S, Gao Y, Chen X, Sui X, et al. The emerging role of ferroptosis in inflammation. *Biomed Pharmacother*. 2020;127:110108. doi: 10.1016/j.biopha.2020.110108
10. Bajic G, Degn SE, Thiel S, Andersen GR. Complement activation, regulation, and molecular basis for complement-related diseases. *EMBO J*. 2015;34:2735-2757. doi: 10.15252/embj.201591881
11. Frid MG, McKeon BA, Thurman JM, Maron BA, Li M, Zhang H, Kumar S, Sullivan T, Laskowsky J, Fini MA, et al. Immunoglobulin-driven Complement Activation Regulates Proinflammatory Remodeling in Pulmonary Hypertension. *Am J Respir Crit Care Med*. 2020;201:224-239. doi: 10.1164/rccm.201903-0591OC
12. Watanabe S, Alexander M, Misharin AV, Budinger GRS. The role of macrophages in the resolution of inflammation. *J Clin Invest*. 2019;129:2619-2628. doi: 10.1172/JCI124615
13. Florentin J, Coppin E, Vasamsetti SB, Zhao J, Tai YY, Tang Y, Zhang Y, Watson A, Sembrat J, Rojas M, et al. Inflammatory Macrophage Expansion in Pulmonary Hypertension Depends upon Mobilization of Blood-Borne Monocytes. *J Immunol*. 2018;200:3612-3625. doi: 10.4049/jimmunol.1701287
14. Prins KW, Thenappan T, Weir EK, Kalra R, Pritzker M, Archer SL. Repurposing Medications for Treatment of Pulmonary Arterial Hypertension: What's Old Is New Again. *J Am Heart Assoc*. 2019;8:e011343. doi: 10.1161/JAHA.118.011343
15. Doll S, Proneth B, Tyurina YY, Panzilius E, Kobayashi S, Ingold I, Irmler M, Beckers J, Aichler M, Walch A, et al. ACSL4 dictates ferroptosis sensitivity by shaping cellular lipid composition. *Nat Chem Biol*. 2017;13:91-98. doi: 10.1038/nchembio.2239
16. Prisco SZ, Eklund M, Raveendran R, Thenappan T, Prins KW. With No Lysine Kinase 1 Promotes Metabolic Derangements and RV Dysfunction in Pulmonary Arterial Hypertension. *JACC Basic Transl Sci*. 2021;6:834-850. doi: 10.1016/j.jacbts.2021.09.004
17. Kazmirczak F, Hartweck LM, Vogel NT, Mendelson JB, Park AK, Raveendran RM, O-Uchi J, Jhun BS, Prisco SZ, Prins KW. Intermittent Fasting Activates AMP-Kinase to Restructure Right Ventricular Lipid Metabolism and Microtubules. *JACC Basic Transl Sci*. 2023;8:239-254. doi: 10.1016/j.jacbts.2022.12.001
18. Meloche J, Pflieger A, Vaillancourt M, Paulin R, Potus F, Zervopoulos S, Graydon C, Courboulin A, Breuils-Bonnet S, Tremblay E, et al. Role for DNA damage signaling in pulmonary arterial hypertension. *Circulation*. 2014;129:786-797. doi: 10.1161/CIRCULATIONAHA.113.006167
19. Alva JA, Zovein AC, Monvoisin A, Murphy T, Salazar A, Harvey NL, Carmeliet P, Iruela-Arispe ML. VE-Cadherin-Cre-recombinase transgenic mouse: a tool for lineage analysis and gene deletion in endothelial cells. *Dev Dyn*. 2006;235:759-767. doi: 10.1002/dvdy.20643

20. Yamamoto K, Lemay SE, Yokokawa T, Breuils-Bonnet S, Salem M, Potus F, Provencher S, Boucherat O, Bonnet S. DNA-Protein Kinase Catalytic Subunit as a Potential Target for Pulmonary Arterial Hypertension. *Am J Respir Cell Mol Biol*. 2023;68:116-119. doi: 10.1165/rcmb.2022-0239LE
21. Pullamsetti SS, Mamazhakypov A, Weissmann N, Seeger W, Savai R. Hypoxia-inducible factor signaling in pulmonary hypertension. *J Clin Invest*. 2020;130:5638-5651. doi: 10.1172/JCI137558
22. Maron BA, Wilkins MR. TORward a Molecular Convergence Point in Pulmonary Arterial Hypertension With mTOR. *JACC Basic Transl Sci*. 2018;3:763-765. doi: 10.1016/j.jacbts.2018.08.003
23. Sutendra G, Michelakis ED. The metabolic basis of pulmonary arterial hypertension. *Cell Metab*. 2014;19:558-573. doi: 10.1016/j.cmet.2014.01.004
24. Lee MH, Sanders L, Kumar R, Hernandez-Saavedra D, Yun X, Ford JA, Perez MJ, Mickael C, Gandjeva A, Koyanagi DE, et al. Contribution of fatty acid oxidation to the pathogenesis of pulmonary hypertension. *Am J Physiol Lung Cell Mol Physiol*. 2022;323:L355-L371. doi: 10.1152/ajplung.00039.2022
25. Bertero T, Oldham WM, Cottrill KA, Pisano S, Vanderpool RR, Yu Q, Zhao J, Tai Y, Tang Y, Zhang YY, et al. Vascular stiffness mechanoactivates YAP/TAZ-dependent glutaminolysis to drive pulmonary hypertension. *J Clin Invest*. 2016;126:3313-3335. doi: 10.1172/JCI86387
26. Wertheim BM, Wang RS, Guillermier C, Hütter CV, Oldham WM, Menche J, Steinhauser ML, Maron BA. Proline and glucose metabolic reprogramming supports vascular endothelial and medial biomass in pulmonary arterial hypertension. *JCI Insight*. 2023;8. doi: 10.1172/jci.insight.163932
27. Kao CC, Wedes SH, Hsu JW, Bohren KM, Comhair SA, Jahoor F, Erzurum SC. Arginine metabolic endotypes in pulmonary arterial hypertension. *Pulm Circ*. 2015;5:124-134. doi: 10.1086/679720
28. Fang X, Wang H, Han D, Xie E, Yang X, Wei J, Gu S, Gao F, Zhu N, Yin X, et al. Ferroptosis as a target for protection against cardiomyopathy. *Proc Natl Acad Sci U S A*. 2019;116:2672-2680. doi: 10.1073/pnas.1821022116
29. Sutendra G, Bonnet S, Rochefort G, Haromy A, Folmes KD, Lopaschuk GD, Dyck JR, Michelakis ED. Fatty acid oxidation and malonyl-CoA decarboxylase in the vascular remodeling of pulmonary hypertension. *Sci Transl Med*. 2010;2:44ra58. doi: 10.1126/scitranslmed.3001327
30. Ryan JJ, Archer SL. Emerging concepts in the molecular basis of pulmonary arterial hypertension: part I: metabolic plasticity and mitochondrial dynamics in the pulmonary circulation and right ventricle in pulmonary arterial hypertension. *Circulation*. 2015;131:1691-1702. doi: 10.1161/CIRCULATIONAHA.114.006979
31. Michelakis ED, Gurtu V, Webster L, Barnes G, Watson G, Howard L, Cupitt J, Paterson I, Thompson RB, Chow K, et al. Inhibition of pyruvate dehydrogenase kinase improves pulmonary arterial hypertension in genetically susceptible patients. *Sci Transl Med*. 2017;9. doi: 10.1126/scitranslmed.aao4583
32. Huertas A, Tu L, Humbert M, Guignabert C. Chronic inflammation within the vascular wall in pulmonary arterial hypertension: more than a spectator. *Cardiovasc Res*. 2020;116:885-893. doi: 10.1093/cvr/cvz308
33. Toshner M, Church C, Harbaum L, Rhodes C, Villar Moreschi SS, Liley J, Jones R, Arora A, Batai K, Desai AA, et al. Mendelian randomisation and experimental medicine approaches to interleukin-6 as a drug target in pulmonary arterial hypertension. *Eur Respir J*. 2022;59. doi: 10.1183/13993003.02463-2020
34. Zamanian RT, Badesch D, Chung L, Domsic RT, Medsger T, Pinckney A, Keyes-Elstein L, D'Aveta C, Spychala M, White RJ, et al. Safety and Efficacy of B-Cell Depletion with Rituximab for the Treatment of Systemic Sclerosis-associated Pulmonary Arterial Hypertension: A Multicenter, Double-Blind, Randomized, Placebo-controlled Trial. *Am J Respir Crit Care Med*. 2021;204:209-221. doi: 10.1164/rccm.202009-3481OC
35. Ferrian S, Cao A, McCaffrey EF, Saito T, Greenwald NF, Nicolls MR, Bruce T, Zamanian RT, Del Rosario P, Rabinovitch M, et al. Single-Cell Imaging Maps Inflammatory Cell Subsets to Pulmonary Arterial Hypertension Vasculopathy. *Am J Respir Crit Care Med*. 2023. doi: 10.1164/rccm.202209-1761OC
36. Asosingh K, Comhair S, Mavrakis L, Xu W, Horton D, Taylor I, Tkachenko S, Hu B, Erzurum S. Single-cell transcriptomic profile of human pulmonary artery endothelial cells in health and pulmonary arterial hypertension. *Sci Rep*. 2021;11:14714. doi: 10.1038/s41598-021-94163-y

37. Xu W, Comhair SAA, Chen R, Hu B, Hou Y, Zhou Y, Mavrakis LA, Janocha AJ, Li L, Zhang D, et al. Integrative proteomics and phosphoproteomics in pulmonary arterial hypertension. *Sci Rep*. 2019;9:18623. doi: 10.1038/s41598-019-55053-6
38. Cracowski JL, Cracowski C, Bessard G, Pepin JL, Bessard J, Schwebel C, Stanke-Labesque F, Pison C. Increased lipid peroxidation in patients with pulmonary hypertension. *Am J Respir Crit Care Med*. 2001;164:1038-1042. doi: 10.1164/ajrccm.164.6.2104033
39. Feng H, Schorpp K, Jin J, Yozwiak CE, Hoffstrom BG, Decker AM, Rajbhandari P, Stokes ME, Bender HG, Csuka JM, et al. Transferrin Receptor Is a Specific Ferroptosis Marker. *Cell Rep*. 2020;30:3411-3423.e3417. doi: 10.1016/j.celrep.2020.02.049
40. Rhodes CJ, Howard LS, Busbridge M, Ashby D, Kondili E, Gibbs JS, Wharton J, Wilkins MR. Iron deficiency and raised hepcidin in idiopathic pulmonary arterial hypertension: clinical prevalence, outcomes, and mechanistic insights. *J Am Coll Cardiol*. 2011;58:300-309. doi: 10.1016/j.jacc.2011.02.057
41. Tatah J, Keen JL, Prisco SZ, Pritzker M, Thenappan T, Prins KW. Iron Deficiency Is Associated With More Severe Pulmonary Vascular Disease in Pulmonary Hypertension Caused by Chronic Lung Disease. *Chest*. 2022;161:232-236. doi: 10.1016/j.chest.2021.07.2159
42. Schuler MH, Di Bartolomeo F, Mårtensson CU, Daum G, Becker T. Phosphatidylcholine Affects Inner Membrane Protein Translocases of Mitochondria. *J Biol Chem*. 2016;291:18718-18729. doi: 10.1074/jbc.M116.722694
43. Kagan VE, Mao G, Qu F, Angeli JP, Doll S, Croix CS, Dar HH, Liu B, Tyurin VA, Ritov VB, et al. Oxidized arachidonic and adrenic PEs navigate cells to ferroptosis. *Nat Chem Biol*. 2017;13:81-90. doi: 10.1038/nchembio.2238
44. Li J, Cao F, Yin HL, Huang ZJ, Lin ZT, Mao N, Sun B, Wang G. Ferroptosis: past, present and future. *Cell Death Dis*. 2020;11:88. doi: 10.1038/s41419-020-2298-2
45. Tamosiuniene R, Manouvakhova O, Mesange P, Saito T, Qian J, Sanyal M, Lin YC, Nguyen LP, Luria A, Tu AB, et al. Dominant Role for Regulatory T Cells in Protecting Females Against Pulmonary Hypertension. *Circ Res*. 2018;122:1689-1702. doi: 10.1161/CIRCRESAHA.117.312058
46. Norlander AE, Abney M, Cephus JY, Roe CE, Irish JM, Shelburne NJ, Newcomb DC, Hemnes AR, Peebles RS. Prostaglandin I. *Am J Respir Crit Care Med*. 2023;208:737-739. doi: 10.1164/rccm.202304-0716LE
47. Perros F, Dorfmüller P, Montani D, Hammad H, Waelput W, Girerd B, Raymond N, Mercier O, Mussot S, Cohen-Kaminsky S, et al. Pulmonary lymphoid neogenesis in idiopathic pulmonary arterial hypertension. *Am J Respir Crit Care Med*. 2012;185:311-321. doi: 10.1164/rccm.201105-0927OC
48. Zhao Q, Song P, Zou MH. AMPK and Pulmonary Hypertension: Crossroads Between Vasoconstriction and Vascular Remodeling. *Front Cell Dev Biol*. 2021;9:691585. doi: 10.3389/fcell.2021.691585
49. Wedgwood S, Lakshminrusimha S, Farrow KN, Czech L, Gugino SF, Soares F, Russell JA, Steinhorn RH. Apocynin improves oxygenation and increases eNOS in persistent pulmonary hypertension of the newborn. *Am J Physiol Lung Cell Mol Physiol*. 2012;302:L616-626. doi: 10.1152/ajplung.00064.2011
50. Wong CM, Preston IR, Hill NS, Suzuki YJ. Iron chelation inhibits the development of pulmonary vascular remodeling. *Free Radic Biol Med*. 2012;53:1738-1747. doi: 10.1016/j.freeradbiomed.2012.08.576
51. Voelkel NF, Tuder RM, Wade K, Höper M, Lepley RA, Goulet JL, Koller BH, Fitzpatrick F. Inhibition of 5-lipoxygenase-activating protein (FLAP) reduces pulmonary vascular reactivity and pulmonary hypertension in hypoxic rats. *J Clin Invest*. 1996;97:2491-2498. doi: 10.1172/JCI118696
52. Hansmann G, Calvier L, Risbano MG, Chan SY. Activation of the Metabolic Master Regulator PPARγ: A Potential PIOneering Therapy for Pulmonary Arterial Hypertension. *Am J Respir Cell Mol Biol*. 2020;62:143-156. doi: 10.1165/rcmb.2019-0226PS
53. Babicheva A, Makino A, Yuan JX. mTOR Signaling in Pulmonary Vascular Disease: Pathogenic Role and Therapeutic Target. *Int J Mol Sci*. 2021;22. doi: 10.3390/ijms22042144
54. Xu J, Wang J, He M, Han H, Xie W, Wang H, Kong H. Dipeptidyl peptidase IV (DPP-4) inhibition alleviates pulmonary arterial remodeling in experimental pulmonary hypertension. *Lab Invest*. 2018;98:1333-1346. doi: 10.1038/s41374-018-0080-1
55. Jones JE, Walker JL, Song Y, Weiss N, Cardoso WV, Tuder RM, Loscalzo J, Zhang YY. Effect of 5-lipoxygenase on the development of pulmonary hypertension in rats. *Am J Physiol Heart Circ Physiol*. 2004;286:H1775-1784. doi: 10.1152/ajpheart.00281.2003

56. Prisco SZ, Hartweck L, Keen JL, Vogel N, Kazmirczak F, Eklund M, Hemnes AR, Brittain EL, Prins KW. Glyoxylase-1 combats dicarbonyl stress and right ventricular dysfunction in rodent pulmonary arterial hypertension. *Front Cardiovasc Med*. 2022;9:940932. doi: 10.3389/fcvm.2022.940932
57. Prisco SZ, Hartweck LM, Rose L, Lima PDA, Thenappan T, Archer SL, Prins KW. Inflammatory Glycoprotein 130 Signaling Links Changes in Microtubules and Junctophilin-2 to Altered Mitochondrial Metabolism and Right Ventricular Contractility. *Circ Heart Fail*. 2022;15:e008574. doi: 10.1161/CIRCHEARTFAILURE.121.008574
58. Mendelson JB, Sternbach JD, Doyle MJ, Mills L, Hartweck LM, Tollison W, Carney JP, Lahti MT, Bianco RW, Kalra R, et al. Multi-omic and multispecies analysis of right ventricular dysfunction. *J Heart Lung Transplant*. 2023. doi: 10.1016/j.healun.2023.09.020
59. Valente AJ, Maddalena LA, Robb EL, Moradi F, Stuart JA. A simple ImageJ macro tool for analyzing mitochondrial network morphology in mammalian cell culture. *Acta Histochem*. 2017;119:315-326. doi: 10.1016/j.acthis.2017.03.001
60. Hong J, Arneson D, Umar S, Ruffenach G, Cunningham CM, Ahn IS, Diamante G, Bhetraratana M, Park JF, Said E, et al. Single-Cell Study of Two Rat Models of Pulmonary Arterial Hypertension Reveals Connections to Human Pathobiology and Drug Repositioning. *Am J Respir Crit Care Med*. 2021;203:1006-1022. doi: 10.1164/rccm.202006-2169OC
61. Avila Cobos F, Alquicira-Hernandez J, Powell JE, Mestdagh P, De Preter K. Benchmarking of cell type deconvolution pipelines for transcriptomics data. *Nat Commun*. 2020;11:5650. doi: 10.1038/s41467-020-19015-

Novelty and Significance

What is known?

- Ferroptosis is a mode of cell death initiated by lipid peroxidation which results from altered mitochondrial function. Ferroptotic death is highly inflammatory as it leads to release of DAMPs that activate the innate immune system
- PAH is a complex disease marked by mitochondrial derangements in endothelial and pulmonary artery smooth muscle cells, immune cell infiltration, and ectopic complement activation, but a mechanism that integrates all these pathogenic phenotypes is lacking.

What new information does this article contribute?

- Small molecule-mediated ferroptosis inhibition mitigates PAH severity even when evaluated in a translational approach, and multi-omic analyses demonstrate ferroptosis promotes PAH by altering the cellular architecture with increases in PASMC and interstitial macrophage relative abundances, restructuring the lung metabolic landscape, and enhancing peri-vascular complement deposition.
- Ferroptotic DAMPs from human PAEC alter human PASMC genetic regulation and impart changes that phenocopy many previously described PASMC phenotypes including disruptions in mitochondrial morphology, suppression of transcripts responsible for DNA repair and metabolism, activation of HIF/mTOR, and heightened proliferation rates.
- Ferroptotic DAMPs from human PAEC activate monocytes and promote a pro-inflammatory phenotype characterized by higher expression of CD86 and CD209 and lower expression of MerTK.
- AAV1-*Acsl4* treatment results in an inflammatory PAH phenotype in rodents with ectopic complement deposition, suggesting endothelial cell ferroptosis may be sufficient to induce pulmonary hypertension.
- SNPs in ferroptotic genes are independently associated with pulmonary hypertension severity in the Vanderbilt BioVU database.